

SPATIALLY RESOLVED OPTICAL IMAGES OF HIGH-REDSHIFT QUASI-STELLAR OBJECTS

TIMOTHY M. HECKMAN,^{1,2,3} MATTHEW D. LEHNERT,^{1,2,4} WIL VAN BREUGEL,^{3,5} AND GEORGE K. MILEY^{2,3,6}

Received 1990 June 21; accepted 1990 August 29

ABSTRACT

We present and discuss the results of a program of deep optical imaging of 19 high-redshift ($z \geq 2$) radio-loud QSOs. These data represent the first large body of nonradio detections of spatially resolved structure surrounding high-redshift QSOs.

In 15 of 18 cases, the Ly α emission is spatially resolved, with a typical size of 100 kpc (for $H_0 = 75 \text{ km s}^{-1} \text{ Mpc}^{-1}$; $q_0 = 0$). The luminosity of the resolved Ly α is $\approx 10^{44} \text{ ergs s}^{-1}$ ($\approx 10\%$ of the total Ly α luminosity). The nebulae are usually asymmetric and/or elongated with a morphological axis that aligns with the radio source axis to better than $\approx 30^\circ$. These properties are quite similar to those of the Ly α nebulae associated with high- z radio galaxies. The brighter side of the nebula is generally on the same side as the brighter radio emission and/or one-sided, jetlike radio structure. There is no strong correlation between the Ly α isophotal and radio sizes (the Ly α nebulae range from several times larger than the radio source to several times smaller). None of the properties of the nebulae correlate with the presence or strength of C IV “associated” absorption ($z_{\text{abs}} \approx z_{\text{em}}$).

It is likely that the nebulae are the interstellar or circumgalactic medium of young or even protogalaxies being photoionized by QSO radiation that escapes anisotropically along the radio axis. Photoionization equilibrium arguments imply that the Ly α emission arises in small (parsec-scale) dense (10^2 – 10^3 cm^{-3}) clouds. If the clouds are not confined, their short lifetime to photoevaporation requires a total reservoir of a few times $10^{11} M_\odot$ in dense gas. If the clouds are confined by a hot, diffuse intercloud medium at the Compton or Virial temperature ($\approx 10^7 \text{ K}$), the mass of this ICM is $\approx 10^{12} M_\odot$. Cloud confinement by a “cocoon” inflated by the radio source or by a thermal QSO wind also entail a substantial total gas mass ($> 10^{11} M_\odot$). The interaction of the radio jet with the ambient gaseous medium may enhance the (radio) visibility of the jet plasma, and lead directly to the small sizes and distorted and asymmetric structures of the radio sources. Indeed, the gas pressures inferred for the Ly α nebulae are far larger than those inferred around low- z radio galaxies and radio-loud QSOs.

For at least six and probably 10 of the QSOs, the UV continuum is also spatially resolved, with diameters of 40–80 kpc. The spatially resolved material is typically $\approx 10\%$ as bright as the QSO, with an average UV luminosity (λP_λ at $\approx 1200 \text{ \AA}$) of $\approx 2 \times 10^{45} \text{ ergs s}^{-1}$ (comparable to the UV luminosities of high- z radio galaxies). The morphological axes of the spatially extended continuum structures do *not* generally align with either the radio or Ly α morphological axes (contrary to the properties of high- z radio galaxies). This UV “fuzz” may be starlight from the QSO host galaxy, scattered QSO light, or even a foreground galaxy acting as a gravitational lens. By analogy to high- z radio galaxies, the first possibility is most likely, implying typical star-formation rates of several hundred M_\odot per year. If sustained for a galaxy dynamical time (several times 10^8 yr) this would result in the formation of a galaxy’s worth of stars. High-redshift radio-loud QSOs may be associated with the formation of some galaxies. Finally, we note that several QSOs have possible close (within 100 kpc of the QSO) companion galaxies with Ly α emission. These require spectroscopic confirmation.

Subject headings: galaxies: interstellar matter — quasars

1. INTRODUCTION

The most fascinating active galactic nuclei (AGNs) are the QSOs at the highest redshifts ($z \geq 2$). First, they are the most luminous objects in the universe and therefore place the most severe demands on theories of the AGN phenomenon. Second, their high luminosities and great distances make them unique

probes of conditions in the early universe. Indeed, luminous QSOs are essentially creatures of the early universe that are nearly extinct today: such QSOs exhibit very strong evolution with cosmic epoch, possibly reaching a maximum co-moving density during the “QSO epoch” at redshifts of ≈ 2 – 3 (Koo, Kron, & Cudworth 1986; Schmidt, Schneider, & Gunn 1986). This strong cosmological evolution is both mysterious and profound: while the bulk of the energy ever produced anywhere by AGNs over the history of the universe was probably produced by high-redshift QSOs (see Soltan 1982; Cavaliere & Padovani 1988), there is still no real understanding of the processes that fostered the QSO epoch.

It is certainly intriguing that current cold dark matter cosmogonies imply that the QSO epoch was also when typical galaxies were hierarchically assembled via dissipative mergers (e.g., Carlberg & Couchman 1989; Carlberg 1990). More generally, Rees (1988) has stressed that in any theory of galaxy for-

¹ Postal address: Rowland Department of Physics and Astronomy, The Johns Hopkins University, Baltimore, MD 21218.

² Space Telescope Science Institute.

³ Visiting observers at the Kitt Peak National Observatory of the National Optical Astronomy Observatories, operated by AURA under contract with the National Science Foundation.

⁴ Astronomy Program, University of Maryland.

⁵ Postal address: Institute for Geophysics and Planetary Physics, Lawrence Livermore Laboratories, L-413, Livermore, CA 94550.

⁶ Postal address: Sterrewacht Leiden, Postbus 9513, 2300RA Leiden, The Netherlands.

mation, significant amounts of infalling gas must have been present around galaxies during the QSO epoch. Rees also argues that such infalling gas will inevitably develop a two-phase structure, with a cool, dense phase ("clouds") that could be highly luminous if irradiated by a QSO at the center of the (proto)galaxy (see also Fall & Rees 1985). Such an infall could fuel the QSO. The irradiation of this infalling material by the QSO might allow us to glimpse the process of galaxy-building (albeit perhaps considerably altered by the effect of the QSO!).

Indeed, optical investigations of high-redshift radio galaxies have revealed objects that conform in many ways to these theoretical expectations. These active galaxies are very luminous in the rest-frame UV continuum, have complex multimodal morphologies, and are associated with large and luminous gaseous nebulae (McCarthy 1988; Chambers 1989). While these characteristics suggest that the radio galaxies may be massive galaxies in the process of forming/assembling, the strong alignment between the radio source axis and the optical major axes (both the gas and continuum emission) implies that there is an intimate connection between the radio source and the structure of the galaxy (Chambers, Miley, & van Breugel 1987; McCarthy et al. 1987b).

The question of how radio-loud QSOs are related to radio galaxies is a topical one and of fundamental importance. Barthel (1989) has proposed that the radio-loud QSOs and radio galaxies are intrinsically the same class of object viewed along or perpendicular to the radio axis, respectively. However, the QSOs and radio galaxies might instead be related in an evolutionary sense (e.g., QSOs represent the periods of maximum nuclear activity in the history of radio galaxies). It is also possible that whether a given AGN becomes a radio-loud QSO or radio galaxy is determined by its environment (e.g., Norman & Miley 1984).

Our understanding of high- z QSOs, and therefore our ability to address these important issues, has been greatly hampered by our nearly complete ignorance concerning their spatial structure or environment. Until very recently, measurements of the sizes and structures of the nonthermal radio sources associated with high- z QSOs have provided the only (albeit indirect) method for obtaining spatially resolved information about physical conditions in the vicinity of high- z QSOs. A decrease in the projected linear sizes of these radio sources as a function of redshift (Miley 1967, 1971; Wardle & Miley 1974) was interpreted as indicating that the gas surrounding radio-loud QSOs became denser at higher redshifts. More recently, the discovery that the QSO radio morphologies may become more distorted at higher redshift provides possible further evidence for the existence of a denser or clumpier medium around high- z radio-loud QSOs (Miley 1987; Barthel & Miley 1988, hereafter BM; but see Neff, Hutchings, & Gower 1989 and Kapahi 1990). In a related vein, Garrington & Conway (1990) find that the amount of Faraday depolarization exhibited by QSO radio sources is a strong function of redshift, probably indicating that the high- z sources are immersed in denser gaseous environments.

Optical imagery of the environments of high- z QSOs has heretofore focused on the detection of companion galaxies, chiefly through their Ly α emission. While the overall success rate has been low, these surveys have led to the discovery of a handful of "Ly α companions" (Djorgovski et al. 1985, 1987; Djorgovski 1988; Hu & Cowie 1987; Hu et al. 1990; Schneider et al. 1987; Spinrad 1987). Hu et al. (1990) conclude that these companions are intimately related to the QSO radio source

phenomenon, being found exclusively in the near neighborhood (≤ 100 kpc or so) of radio-loud QSOs.

Motivated by the arguments and results summarized above, we have undertaken an optical imaging survey of 19 high-redshift, radio-selected QSOs in the light of the H I Ly α emission line and the rest-frame UV continuum. We have discovered spatially resolved Ly α emission in 15 of them and spatially resolved continuum emission in at least six, and probably 10.

2. SAMPLE SELECTION, OBSERVATIONS, AND ANALYSIS

2.1. *The Sample*

The sample of QSOs we observed are listed in Table 1, together with most of their salient properties. We have exclusively observed radio-loud QSOs whose radio emission arises on large scales (≈ 10 kpc to several hundred kpc) rather than radio-quiet QSOs or QSOs with predominantly ultracompact radio emission. We have done so for a variety of reasons. First, this is precisely the class for which the radio data suggest a dense gaseous environment (see above). Second, radio galaxies at similar redshifts and with similar radio properties are commonly enveloped in large, bright, emission-line nebulae and are relatively bright, spatially extended UV-continuum sources as well (see McCarthy 1988; Chambers 1989). Third, at low redshifts ($z \leq 0.5$) this subclass of QSO has much brighter and more spatially extended emission-line gas than other QSO types (Stockton & MacKenty 1987; Boroson, Persson, & Oke 1985), and is associated with exceptionally luminous host galaxies (Smith et al. 1986). Indeed, Crawford & Fabian (1989, hereafter CF) have investigated bright emission-line nebulae around eight radio-loud QSOs with $z \approx 0.4-0.9$. Finally, Foltz et al. (1988) argued that QSOs with powerful, large-scale radio emission preferentially have a higher incidence rate of narrow C IV absorption lines within 5000 km s^{-1} of the QSO redshift than other QSO classes. While the reality of this effect has been disputed by Sargent, Boksenberg, & Steidel (1988), it is potential evidence for an unusual amount of gas somewhere in the vicinity of radio-loud QSOs.

2.2. *Observations and Calibration*

Our data consist of images obtained with the UV-flooded TI2 CCD at the Prime Focus of the KPNO 4 m telescope during 1988 May and November. The CCD was used in its full 800×800 pixel mode (no on-chip summation) yielding $0''.3$ pixels and a $4'$ field. The Ly α images were taken through narrow-band interference filters (FWHM $\approx 60 \text{ \AA}$) purchased by one of us (W. v. B.) in collaboration with H. Spinrad. These images had total integration times of 1–2 hr (see Table 1). We also obtained continuum images with typically 10 minute exposure times through a broad-band filter (U or B) having an effective wavelength within several hundred angstroms of the corresponding Ly α filter (see Table 1 for details). The signal level reached in the sky was in all cases well above the faint regime in which the TI CCDs suffer from poor charge transfer, so no preflashing was necessary. Observing conditions were generally good [photometric, typical sky brightness $\approx 21.7(U)$ and $\approx 22.1(B)$ mag arcsec $^{-2}$, and seeing $\approx 1''.2 \pm 0''.3$ FWHM; see Table 1].

The data were flat-fielded in the conventional way: a two-dimensional bias frame was subtracted from all the frames which were then divided by a normalized image taken through the appropriate filter of a dome screen illuminated by a quartz lamp. We then used the task "BACKGROUND" in IRAF to

TABLE 1
SAMPLE AND OBSERVATIONS

QSO (1)	z (2)	Narrow-Band Filter (3)	Exposure (4)	Point Spread Function (5)	Broad-Band Filter (6)	Exposure (7)	Point Spread Function (8)	Date (1988) (9)
Q0017+154.....	2.012	3662/60	3600	0.8	<i>U</i>	600	0.8	Nov 10
Q0109+176.....	2.157	3875/60	3600	1.2	<i>U</i>	600	1.4	Nov 11
Q0225-014.....	2.037	3734/60	3600	0.8	<i>U</i>	600	0.8	Nov 13
Q0316-203.....	2.880	4710/60	3600	1.2	<i>B</i>	600	1.2	Nov 11
Q0445+097.....	2.110	3807/60	3600	0.9	<i>U</i>	600	0.9	Nov 13
Q0549-213.....	2.245	<i>U</i>	4200	1.2	Nov 13
Q0730+257.....	2.686	4479/60	3600	1.6	<i>B</i>	600	1.8	Nov 11
Q0751+298.....	2.106	3807/60	3600	1.5	<i>U</i>	600	1.5	Nov 13
Q0758+120.....	2.660	4479/60	3600	1.4	<i>B</i>	600	1.4	Nov 11
Q0805+046.....	2.877	4710/60	3600	1.0	<i>B</i>	600	1.0	Nov 12
Q0941+261.....	2.910	4743/60	3600	1.0	<i>B</i>	600	1.3	Nov 13
Q1318+113.....	2.171	3870/60	7168	1.4	<i>B</i>	640	1.4	May 15
Q1345+584.....	2.039	3700/100	3584	1.5	<i>B</i>	512	1.4	May 13
Q1354+258.....	2.032	3700/100	7168	1.2	<i>B</i>	512	1.4	May 13
Q1658+575.....	2.173	3870/60	5376	1.2	<i>B</i>	512	1.2	May 12
Q2150+053.....	1.979	3662/60	3600	1.0	<i>U</i>	600	1.2	Nov 12
Q2222+051.....	2.323	4043/60	4200	1.0	<i>B</i>	540	1.4	Nov 10
Q2251+244.....	2.328	4043/60	3600	1.2	<i>B</i>	600	1.6	Nov 10
Q2338+042.....	2.594	4360/50	3600	1.2	<i>B</i>	600	1.2	Nov 13

Col. (2).—Redshift taken from the Hewitt & Burbidge 1987 compilation.

Col. (3).—The nominal central wavelength and width (in angstroms) of the narrow-band filter used to image redshifted Ly α . Note that the effective central wavelength of these filters in the $f/2.7$ beam at prime focus on the KPNO 4 m telescope is ~ 15 Å blueward of the nominal values given in this table.

Col. (4).—The exposure time in the narrow-band images (in seconds).

Col. (5).—The FWHM of the point-spread function in the narrow-band image (in arcseconds).

Col. (6).—The broad-band filter (from the KPNO “nearly Mould” set) used for the continuum image.

Cols. (7) and (8).—As in cols. (4) and (5), but for the broad-band images.

fit and remove the sky on a row-by-row basis with a third-order Chebychev polynomial. This process effectively removed residual $\approx 1\%$ amplitude low-spatial-frequency errors in the initial flat-fielding. The data were then flux-calibrated using observations of KPNO IRS/IIDS and Landolt standard stars made at the beginning and end of each night. The standard KPNO extinction correction was applied to calculate the fluxes above the atmosphere.

2.3. Image Analysis

After flat-fielding, the images were processed in several independent ways. First, each broad-band image was spatially aligned with its corresponding narrow-band image, and then scaled such that bright stars and galaxies in the broad-band frame had the same total counts as in the narrow-band frame. The difference of the two frames thus contains only the Ly α emission. We will henceforth refer to these as continuum-subtracted (CS) Ly α images.

Second, we used the brightest unsaturated stars in each Ly α and continuum frame to determine the amount of spatially resolved structure around the QSO. We have done this by scaling a star so that it had the same flux in a $1''.5 \times 1''.5$ box as the QSO, shifting the star spatially to align it with the QSO, and then subtracting it from the QSO. This is an overly conservative approach because it assumes that all the QSO flux within a $1''.5$ box arises from a fully unresolved source. We will henceforth refer to these as point-source-subtracted (PSS) Ly α and continuum images. To search for low surface-brightness emission, we convolved the PSS and CS images with a 4×4 pixel median filter and/or a Gaussian with a FWHM of 3.5 pixels (i.e., comparable to the FWHM of the PSF).

Third, to further verify that the QSOs are spatially resolved, we have used the program described in Smith et al. (1986) to

generate azimuthally averaged one-dimensional radial surface brightness profiles (RSB profiles) of the QSOs and bright stars in the Ly α and continuum frames. These were constructed after excising bad columns, cosmic-ray hits, or stars/galaxies near the QSOs or the stars used for the PSF. We can then explicitly compare each RSB profile (Ly α or continuum) to the corresponding PSF.

To check whether there were significant focus variations across the CCD frame, we have constructed multiple PSFs using several bright, but unsaturated stars in each frame. No significant PSF variations were found. We also emphasize that the QSOs were not always positioned at the same location within the CCD frame, and so the QSOs have not somehow been systematically located in a region of the chip having poorer-than-average image quality. Finally, we note that while several of the QSOs are only marginally resolved (i.e., have RSB profiles only slightly more extended than the PSF), there are no cases in which any PSF is more extended than a QSO RSB profile.

We consider spatially extended structures in the Ly α images to be real *only* if they are clearly present in both the CS and PSS frames and if the RSB profile of the QSO is clearly broader than the PSF. The CS images are sensitive to differences in the point-spread function (PSF) between the broad and narrow-band images, including the presence of faint “ghost” images visible in several of the latter. The PSS images circumvent these problems but will still contain any continuum emission that was transmitted by the narrow-band filters. In general, the agreement between the CS and PSS frames is excellent. Moreover, the QSOs deemed to be spatially extended on the basis of inspection of these two-dimensional CS and PSS images were also resolved in the one-dimensional RSB profile versus PSF comparisons.

We are therefore confident that we have detected spatially extended emission around ~ 15 of the 18 QSOs for which we have Ly α images (see Tables 1 and 2) and around at least six and probably 10 of the 18 cases for which we have continuum (U or B) frames and can measure the PSF (see Table 3).

We have then measured the total fluxes, the spatially extended fluxes (in the PSS images), and the diameters at the faintest detectable isophotal level: few times 10^{-17} ergs cm^{-2} s^{-1} arcsec $^{-2}$ in the Ly α frames and $\approx 1\%$ of sky (≈ 27 mag arcsec $^{-2}$) in the continuum frames. Comparison of the night-to-night and intra-night standard star observations imply that purely photometric errors are small ($< 10\%$). However, the uncertainties in the exact placements of the Ly α line emission within the interference filters' narrow bandpasses (owing chiefly to the uncertain redshift of the spatially extended Ly α emission) lead to potentially larger uncertainties in the true Ly α fluxes (up to 30% for gas within ≈ 1500 km s^{-1} of the published QSO redshift). The largest source of uncertainty in the fluxes of the *spatially extended* Ly α and continuum emission arise from the ambiguities in the "point-source" versus "fuzz" deconvolution. As noted above, we have probably systematically underestimated the fluxes by assuming that the central $1''.5$ is pure QSO light. From repeated iterative attempts to satisfactorily align, scale, and subtract the central QSO in the PSS images, we estimate that the uncertainties produced by

this process range from 0.1 to 0.3 dex depending on the degree of resolution (see Tables 2 and 3 for specifics). The uncertainties in the Ly α isophotal diameters are ≈ 0.1 – 0.2 dex except in a few marginally resolved cases (see Table 2 for specifics). The spatially resolved continuum structures tend to be more compact than the Ly α , and the uncertainties in the isophotal radii resulting from the QSO subtraction procedure are therefore larger (0.2–0.3 dex).

We have used our Ly α images to correct the fluxes of the spatially extended continuum structures for the presence of Ly α emission transmitted through the U or B filter bandpass. Spatially resolved Ly α line emission usually makes only a minor ($\approx 10\%$) contribution to the spatially resolved continuum emission, with significantly larger fractions occurring in Q0805+046 (50%) and Q2338+042 (30%). Thus, the properties of the continuum structures in these two QSOs are particularly uncertain.

We have calculated luminosities and linear diameters for an $H_0 = 75$ km s^{-1} Mpc $^{-1}$ and $q_0 = 0$ cosmological model. For our typical redshifts (median $z \approx 2.3$), these parameters have values quite close to those implied by an $H_0 = 50$ and $q_0 = 0.5$ cosmological model. Within the full range of plausible cosmological parameters ($H_0 = 50$ – 100 km s^{-1} Mpc $^{-1}$ and $q_0 = 0$ – 0.5) the implied linear sizes could vary from ~ 0.5 – 1.5 times our adopted values, and the implied luminosities could vary

TABLE 2
PROPERTIES OF THE Ly α NEBULAE

QSO (1)	z (2)	$\log F_{\text{Ly}\alpha}$ (3)	$\log L_{\text{Ly}\alpha}$ (4)	$\log R$ (5)	$\theta_{\text{Ly}\alpha}$ (6)	$D_{\text{Ly}\alpha}$ (7)
Q0017+154	2.012	−14.4b	44.1	−0.7	11a	97
Q0109+176	2.157	−15.4c	43.2	−1.1	3b	26
Q0225−014	2.037	−14.8c	43.8	−1.2	5?	43
Q0316−203	2.88	<−15.7	<43.3	<−1.3
Q0445+097	2.11	−14.7a	44.2	−0.2	12a	100
Q0730+257	2.686	−15.1c	43.9	−1.0	11b	99
Q0751+298	2.106	<−15.0	<43.6	<−1.3
Q0758+120	2.66	−14.8a	44.1	−0.3	13a	120
Q0805+046	2.877	−14.1b	44.9	−0.6	14a	130
Q0941+261	2.91	−15.1c	43.9	−1.0	12b	110
Q1318+113	2.171	−14.2b	44.4	−0.6	11a	96
Q1345+584	2.039	−14.1c	44.4	−1.0	9b	79
Q1354+258	2.032	−14.2b	44.3	−0.6	9a	79
Q1658+575	2.173	−14.5c	44.1	−1.0	10b	88
Q2150+053	1.979	−14.8c	43.7	−1.1	10b	87
Q2222+051	2.323	−14.8b	44.0	−0.8	12a	107
Q2251+244	2.328	<−15.7	<43.3	<−1.3
Q2338+042	2.594	−14.6b	44.3	−0.5	11a	100
Median	2.2	−14.7	44.0	−1.0	11	97

COL. (3).—The log of the *spatially resolved* Ly α flux (cgs units), as measured from the point-source-subtracted (PSS) images; see text for details. The uncertainties are usually dominated by uncertainties in the deconvolution into QSO and nebular light, and are coded as follows: $a = 0.1$ dex, $b = 0.2$ dex, $c = 0.3$ dex.

COL. (4).—The log of the *spatially resolved* Ly α luminosity (ergs s^{-1}), calculated for our adopted cosmology of $H_0 = 75$ km s^{-1} Mpc $^{-1}$ and $q_0 = 0$. These luminosities have been corrected for Galactic extinction using the extinction maps of Burstein & Heiles 1982 and the reddening law in Osterbrock 1989. The uncertainties in these luminosities are the same as given in col. (3) for the fluxes.

COL. (5).—The log of the ratio of the (spatially extended/total) Ly α emission in our images. The uncertainties are given in col. (3).

COL. (6).—The maximum angular size of the Ly α nebula (in arcseconds). This is typically measured at a surface brightness level of ≈ 2 – 3×10^{-17} ergs cm^{-2} s^{-1} arcsec $^{-2}$ in the Earth's frame, or a factor of typically 100 times higher in the QSO rest frame. Sizes coded by "a" are uncertain by ~ 0.1 dex, sizes coded by "b" are uncertain by 0.2 dex, and sizes coded " ? " are only marginally resolved.

COL. (7).—The maximum linear extent of the nebula (in kiloparsecs). The uncertainties are given in col. (7).

TABLE 3
CONTINUUM PROPERTIES OF THE QSOs

QSO (1)	m (2)	λ_0 (3)	$\log P_{\lambda 0}$ (4)	$\log L_{\text{tot}}$ (5)	$\log L_{\text{fuzz}}$ (6)	D_{fuzz} (7)
Q0017+154	17.4(U)	1230	43.7	46.8	<45.3	...
Q0109+176	18.5(U)	1170	43.3	46.4	<44.9	...
Q0225-014	17.9(U)	1220	43.4	46.5	45.2c	5; 43
Q0316-203	19.9(B)	1130	43.4	46.4	<44.9	...
Q0445+097	20.2(U)	1190	42.9	46.0	45.6a	8; 66
Q0549-213	19.6(U)	1140	43.0	46.0	45.3b	7; 62
Q0730+257	19.6(B)	1190	43.4	46.5	45.1c	7; 63
Q0751+298	17.6(U)	1190	43.6	46.7	<45.2	...
Q0758+120	19.5(B)	1200	43.4	46.5	<45.0	...
Q0805+046	18.7(B)	1130	43.8	46.9	45.5?	9; 83
Q0941+261	18.9(B)	1120	43.8	46.9	<45.4	...
Q1318+113	19.1(B)	1380	43.2	46.3	45.5b	9; 78
Q1345+584	18.6(B)	1440	43.4	46.6	?	...
Q1354+258	18.9(B)	1450	43.1	46.3	44.8?	7; 62
Q1658+575	18.4(B)	1380	43.5	46.6	45.4c	9; 80
Q2150+053	17.6(U)	1240	43.6	46.7	45.2?	?
Q2222+051	19.1(B)	1320	43.4	46.6	<45.1	...
Q2251+244	18.5(B)	1320	43.7	46.8	<45.3	...
Q2338+042	20.3(B)	1220	43.0	46.1	45.3?	6; 55
Median	18.8	1220	43.4	46.5	45; 45.3	≈ 63 kpc

COL. (2).—The broad-band magnitude measured in our images (U or B , as noted in parentheses). The uncertainties are ≈ 0.1 mag.

COL. (3).—The effective central wavelength (in angstroms, in the QSO frame) of the broad-band image. We have taken the effective central wavelengths of the U and B filters (as used with the UV-flooded TI2 CCD) to be 3700 and 4390 Å, respectively.

COL. (4).—The log of the total (QSO + fuzz) monochromatic power ($\text{ergs s}^{-1} \text{Å}^{-1}$) of the continuum at the wavelength given in col. (3). We have calculated these powers after correction for $\text{Ly}\alpha$ emission in the bandpass of the U or B filter. The powers also include corrections for Galactic extinction (see notes to Table 2).

COL. (5).—Log of the total luminosity (QSO + fuzz) of the UV continuum (ergs s^{-1}), taken to be λP_{λ} where λ is from col. (3) and P_{λ} is from col. (4).

COL. (6).—The log of the UV luminosity of the spatially extended continuum emission (fuzz), with luminosity defined as in col. (5). The upper limits given for eight QSOs are based on the faintest fuzz detected in the other QSOs. We had no star suitable to determine the PSF for Q1345+584. For most of the QSOs, the uncertainty in this quantity is dominated by uncertainty in the deconvolution of the image into a QSO and “fuzz” component. However, in Q0805+046 and Q2338+042 the spatially extended $\text{Ly}\alpha$ emission makes significant contributions to the spatially extended emission in the broad-band images ($\approx 50\%$ and $\approx 30\%$, respectively). This makes the properties of “fuzz” in these two QSOs particularly uncertain. Uncertainties are coded as follows: “a” (uncertain by 0.1 dex), “b” (uncertain by 0.2 dex), “c” (uncertain by 0.3 dex), and “?” (marginally resolved and/or strong $\text{Ly}\alpha$ contamination of the image). The two entries under the row for “Median” are for the ensemble of 18 QSOs and for the 10 QSOs with detected fuzz, respectively.

COL. (7).—The maximum detectable diameter of the fuzz (in arcsec; kpc), measured at a limiting surface brightness of $\approx 1\%$ of sky ≈ 27 mag arcsec $^{-2}$. Uncertainties in this quantity are similar to those given in col. (6).

from ~ 0.25 – 2.2 times our adopted values. All the luminosities have been corrected for Galactic extinction using the reddening maps of Burstein & Heiles (1982) and the standard interstellar extinction law (e.g., Osterbrock 1989).

3. RESULTS

3.1. $\text{Ly}\alpha$ Nebulosity

The 15 spatially resolved $\text{Ly}\alpha$ images are shown in Figure 1. We have summarized the properties of the $\text{Ly}\alpha$ nebulae in Table 2, and descriptions of the individual nebulae are given in the Appendix.

Because the images in Figure 1 are generally the CS images (and so have had a scaled version of the U or B frame subtracted), the effective PSFs for the CS images are not the same as (and will be somewhat worse than) the PSFs determined from stars in the original $\text{Ly}\alpha$ frames. The images in Figure 1 are therefore primarily meant to provide morphologi-

cal information. The quantitative evidence that the QSOs are indeed resolved is contained in Figure 2, which for each of the 18 QSOs shows the RSB profile of the $\text{Ly}\alpha$ measured in the original $\text{Ly}\alpha$ image (not the CS image) overlaid on the PSF measured in the same image.

The nebulae have typical diameters of 100 kpc ($\approx 10''$), at isophotal levels of $\sim 2 \times 10^{-17}$ ergs cm $^{-2}$ s $^{-1}$ arcsec $^{-2}$ in $\text{Ly}\alpha$. Note that the surface brightnesses in the QSO rest frame are $(1+z)^4 \approx 100$ times higher than those we measure. The spatially resolved emission has a typical luminosity of $\approx 10\%$ – 25% of the total imaged $\text{Ly}\alpha$ emission. The bulk of the total imaged emission comes from the central, bright unresolved component (the QSO proper). Most of this central emission probably arises in the QSOs broad-line region (BLR). Based on the $\text{Ly}\alpha$ emission-line profiles for the QSOs in our sample (Barthel, Tytler, & Thomson 1990, hereafter BTT; Lehnert et al. 1990a), we estimate that $\sim 50\%$ of the BLR $\text{Ly}\alpha$ emission would have fallen outside the bandpass of the narrow-band

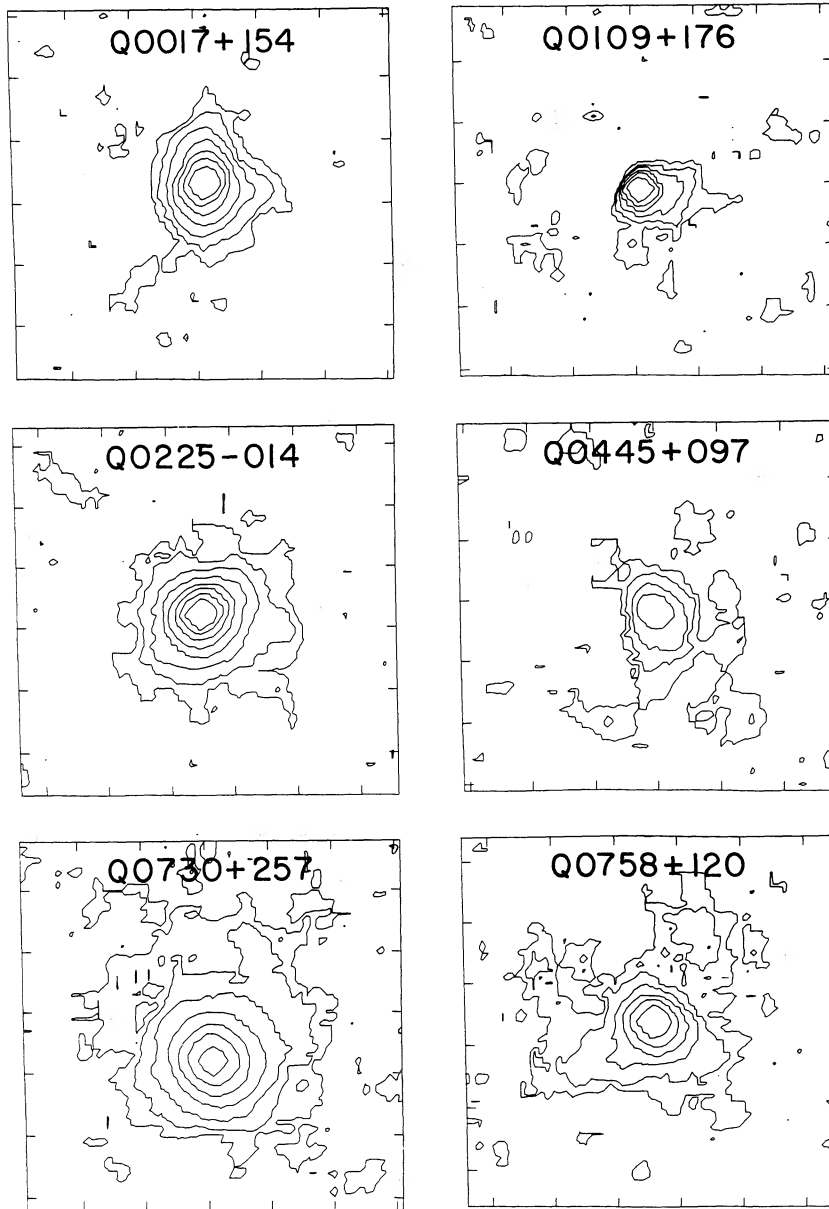


FIG. 1.—Contour plots of the Ly α images of the 15 high- z QSOs with spatially resolved Ly α emission. The images of Q1345+584, Q1354+258, and Q1658+575 have had the spatially unresolved Ly α emission from the QSO proper subtracted at a position indicated by the cross (they are the “PSS” images; see § 2.2). The other images have had the continuum subtracted, but not the Ly α from the central QSO (they are the “CS” images, see § 2.2). Each image is $18'' \times 18''$ arcsec in size with north to the top and east to the left. The value of the lowest contour level (in units of 10^{-17} ergs cm^{-2} s^{-1} arcsec $^{-2}$) is given in Table 5. Each successive contour represents an increase of a factor of 2 in surface brightness. These images have been smoothed with a 4×4 pixel median filter to highlight low-surface brightness emission and to minimize the effects of cosmic rays and “hot” pixels.

filters we employed. Adopting this factor of 2 correction, the Ly α nebulae typically account for $\approx 10\%$ of the total Ly α luminosity.

The amount of morphological information on the nebulae is obviously limited. The majority of the nebulae are rather asymmetric, with most or all of the extended emission arising from “plumes” or “knots” on one side of the QSO. There are also examples with more complex morphologies like Q0758+120 with its multiple filaments, Q0941+261 with its lumpy, multimodal structure, and Q1345+584 with its abrupt change in the position angle of the nebulae between the inner and outer structures (see the Appendix for details).

To put these Ly α nebulae into perspective, it is useful to compare them to the most spectacular emission-line nebulae in our “local” universe (e.g., at $z < 0.2$). These are the optical emission-line nebulae associated with “cooling flows” centered on the dominant galaxy in some clusters of galaxies (see, e.g., Heckman et al. 1989; Hu 1988) and the nebulae associated with powerful radio galaxies (see Baum & Heckman 1989a, b). The most luminous known cooling flow nebulae have Ly α luminosities of several times 10^{42} ergs s^{-1} , while more typical cases have luminosities of one-to-several times 10^{41} ergs s^{-1} . As in the case of our QSO nebulae, these luminosities have been corrected only for foreground extinction in the Milky

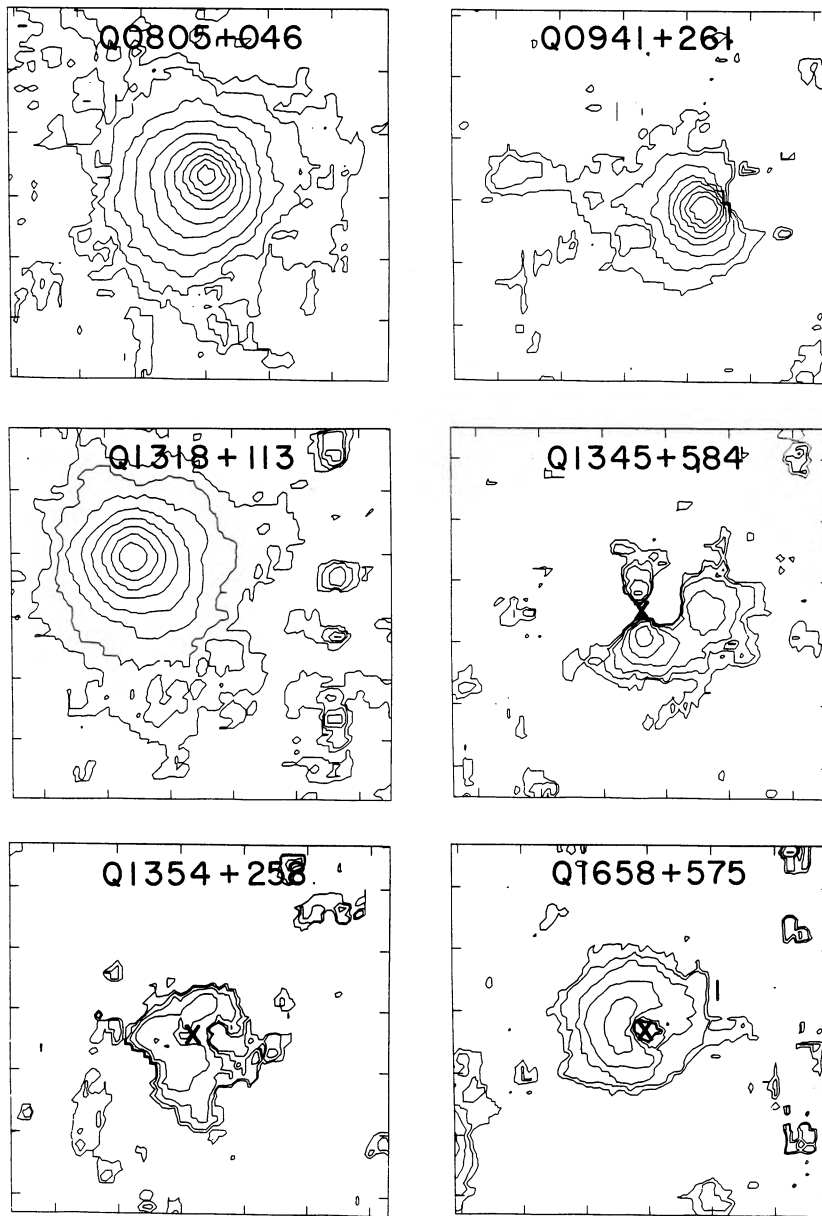


FIG. 1—Continued

Way. The most luminous nebulae associated with low- z radio galaxies have extra-nuclear $H\alpha$ luminosities of several times 10^{41} ergs s^{-1} (where we have included only the emission arising further than 5 kpc from the nucleus since this is the only material we could resolve in our QSO images). The $Ly\alpha$ luminosities of these nebulae can be at most ≈ 10 times larger than the $H\alpha$ luminosities (if the nebulae contain no dust). Thus, the most luminous known emission-line nebulae in the present universe are at least one to two orders of magnitude less luminous in $Ly\alpha$ than the nebulae associated with the high-redshift QSOs.

At slightly higher redshifts ($z \approx 0.2-0.5$), Stockton & Mackenty (1987) have discovered large, luminous emission-line nebulae associated with ten QSOs with strong, extended radio emission. These have extranuclear ($r > 10$ kpc) $[O III] \lambda 5007$ luminosities of typically a few times 10^{42} ergs s^{-1} . The spectra of these nebulae (e.g., Boroson, Persson, & Oke 1985) show

that the $[O III]/H\beta$ flux ratio ≈ 10 . For normal case B conditions then $L_{Ly\alpha} \leq 3 * L_{5007}$ with the equality holding in the unlikely event that there is no dust extinction associated with the nebula (see also Hu et al. 1990 who find $L_{Ly\alpha} \leq 3L_{[O III]}$ in the nebula around the low- z QSO radio-loud QSO 4C 37.43). The low- z QSO nebulae then have $Ly\alpha$ luminosities that are typically more than an order-of-magnitude less than our high- z QSOs. While Hu et al. (1990) find that the luminosities of the “ $Ly\alpha$ companions” near four high- z radio-loud QSOs are similar to the luminosities of the nebulae around low- z radio-loud QSOs, these former luminosities include only the emission from discrete, detached $Ly\alpha$ “knots” near the high- z QSOs. They have not numerically deconvolved the $Ly\alpha$ images into spatially resolved and spatially unresolved components as we have done, and so may be missing a substantial portion of the spatially resolved $Ly\alpha$ emission.

It is especially relevant to compare the properties of the

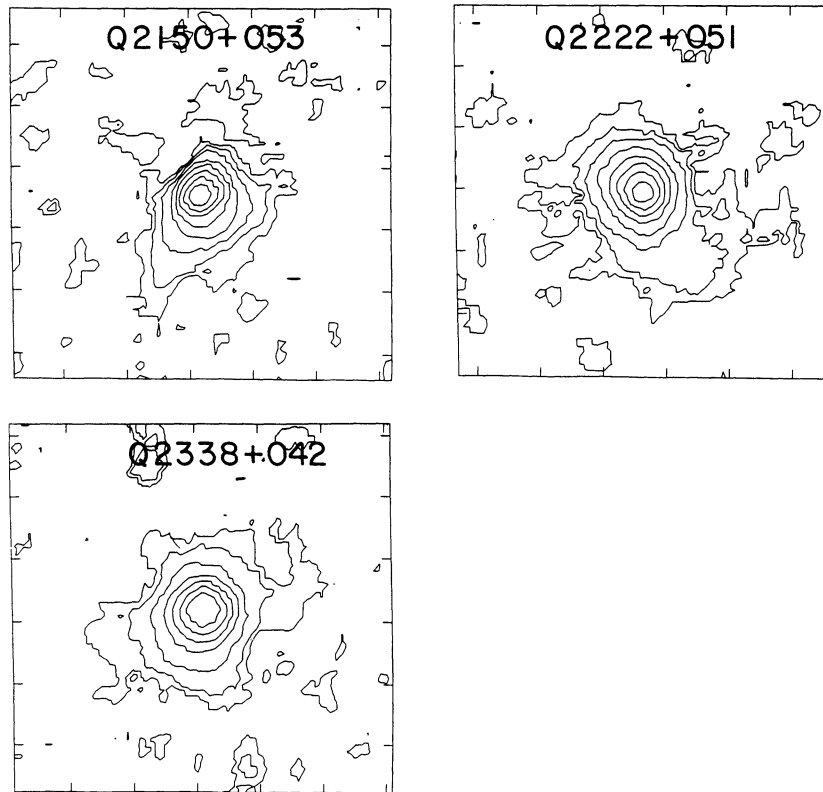


FIG. 1—Continued

nebulae associated with our high- z QSOs to those of radio galaxies with similar redshifts and radio powers (McCarthy et al. 1987a; Chambers, Miley, & van Breugel 1987; McCarthy 1988; Chambers 1989). While the *total* $\text{Ly}\alpha$ luminosities of our QSOs (including the nucleus) are typically an order of magnitude larger than those of the high- z radio galaxies, the luminosities and sizes of the *spatially extended* material are similar in the two classes (cf. Fig. 3).

Taking our QSO sample by itself we find no correlation between the $\text{Ly}\alpha$ and radio luminosities (see Fig. 3). However, if we consider the nebulae in the broader context of radio galaxies and radio-loud QSOs as a whole, the high- z QSOs do lie at the upper end of the broad correlation between radio and emission-line luminosity discussed by Baum & Heckman (1989b) and McCarthy (1988). The $\text{Ly}\alpha$ luminosities of the QSO nebulae are typically several percent of the total radio luminosities (the latter taken to be $\approx 10\nu P_\nu$).

A morphological relationship between the emission-line gas and the nonthermal radio plasma might be expected by analogy to the situation in high redshift radio galaxies (McCarthy et al. 1987b; Chambers, Miley, & van Breugel 1987). Because the QSO radio sources are often highly distorted, we have taken the position angle of the radio axis to be that of the line joining the outer radio hotspots (this circumvents the ambiguity caused by the frequently bent or curved radio structure). Two of us (T. H. and G. M.) have independently measured the position angle of the morphological major axis of the $\text{Ly}\alpha$. Taking the average value, we then find that in nearly every case for which we can make a comparison, the emission-line gas aligns to within $\sim 30^\circ$ with the radio axis (Fig. 4 and Table 4). Since the measuring errors in the $\text{Ly}\alpha$ position angles are typically $\sim 20^\circ$, the true radio- $\text{Ly}\alpha$ align-

ment may be even better than Figure 4 would imply. The only clearly misaligned case is Q2150 + 053. In Q0758 + 120 the $\text{Ly}\alpha$ nebulae is morphologically complex (making it difficult to define “the” $\text{Ly}\alpha$ position angle), while in Q1345 + 584 the outer $\text{Ly}\alpha$ structure aligns well with the radio source, but there is a possible inner $\text{Ly}\alpha$ structure that is roughly orthogonal to the radio axis. The $\text{Ly}\alpha$ nebula in Q1658 + 575 is quite round and no major axis position angle can be assigned. We have omitted these last three QSOs from Figure 4.

We find no overall correlation between the $\text{Ly}\alpha$ isophotal sizes and the radio sizes, in agreement with the results of Baum & Heckman (1989b) and McCarthy (1988) for other extragalactic radio sources. In fact, the log of the ratio of the $\text{Ly}\alpha$ -to-radio size is distributed rather uniformly between -0.7 and $+0.9$. It is interesting, however, that the three QSOs (Q0316 – 203, Q0751 + 298, and Q2251 + 244) with the smallest radio sizes (subarcsec scale) are also the only three QSOs without spatially resolved $\text{Ly}\alpha$ nebosity. This suggests a physical relationship between the presence of large-scale $\text{Ly}\alpha$ and radio-synchrotron plasmas, but a larger sample of QSOs with compact radio sources is needed to substantiate this.

As noted above, the $\text{Ly}\alpha$ nebulae are usually rather asymmetric in morphology. This $\text{Ly}\alpha$ “sidedness” is clearly related to asymmetries in the radio source structure. Of the 15 $\text{Ly}\alpha$ nebulae, there are 10 cases in which the $\text{Ly}\alpha$ and radio sidedness can be well determined (we exclude Q0017 + 154 and Q1658 + 575 which are quite symmetric in $\text{Ly}\alpha$, Q0225 – 014 which is marginally resolved and apparently symmetric in $\text{Ly}\alpha$, Q0758 + 120 which has a morphologically complex $\text{Ly}\alpha$ nebula, and Q1354 + 258 which has a complex radio structure and no clearly defined $\text{Ly}\alpha$ “side”). We then find that the side of the nebula on which the $\text{Ly}\alpha$ is brighter is the same side on

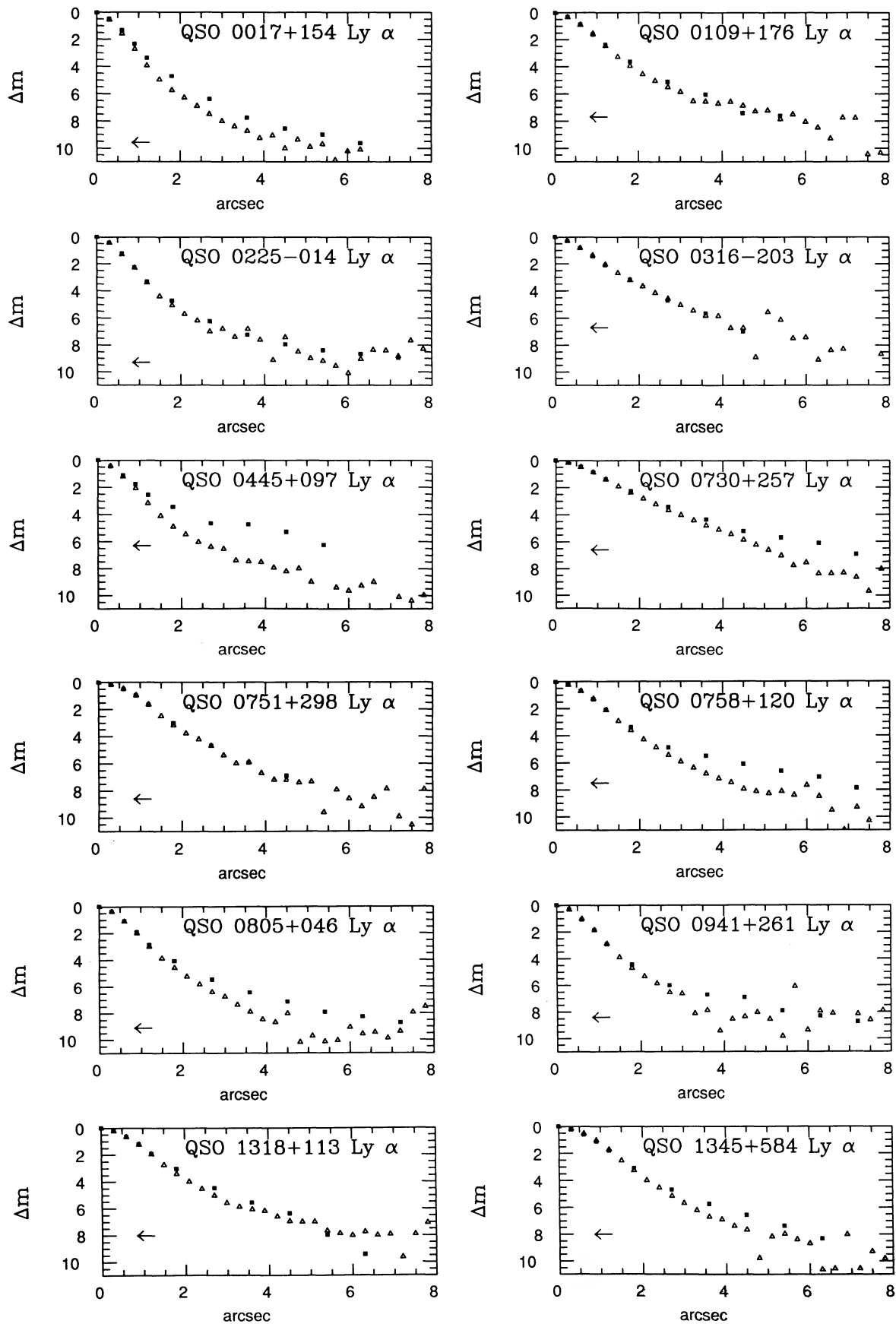


FIG. 2.—Comparison of the azimuthally averaged radial surface brightness profiles (RSBPs) of our sample of 18 QSOs (solid squares) and the point spread functions (PSFs) as measured with bright stars (open triangles) in the narrow-band Ly α images. The surface brightnesses are given in magnitudes relative to the brightest central pixel. The RSBPs are reliable down to a level of $\approx 1\%$ of the sky brightness (level indicated by a horizontal arrow in each plot). Note that in no case is the PSF broader than the RSBP, while the reverse is true in 15 of the 18 QSOs.

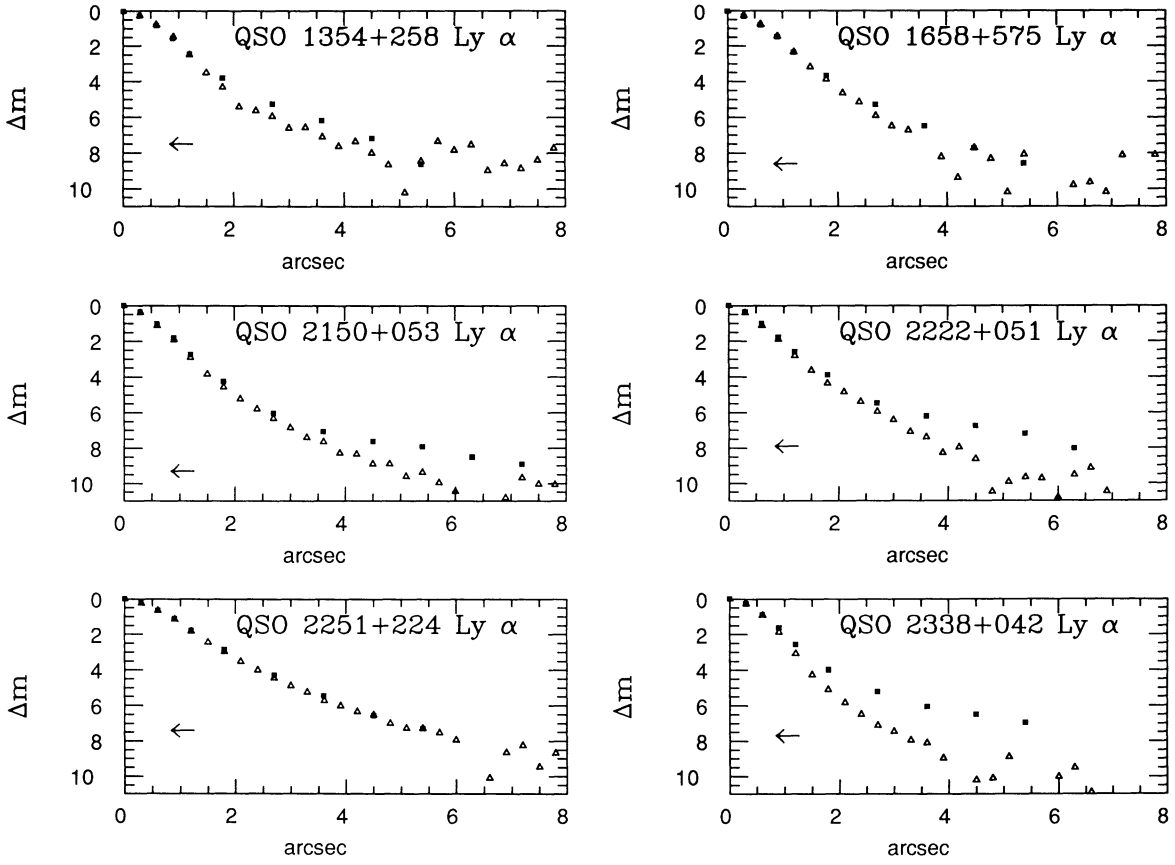


FIG. 2—Continued

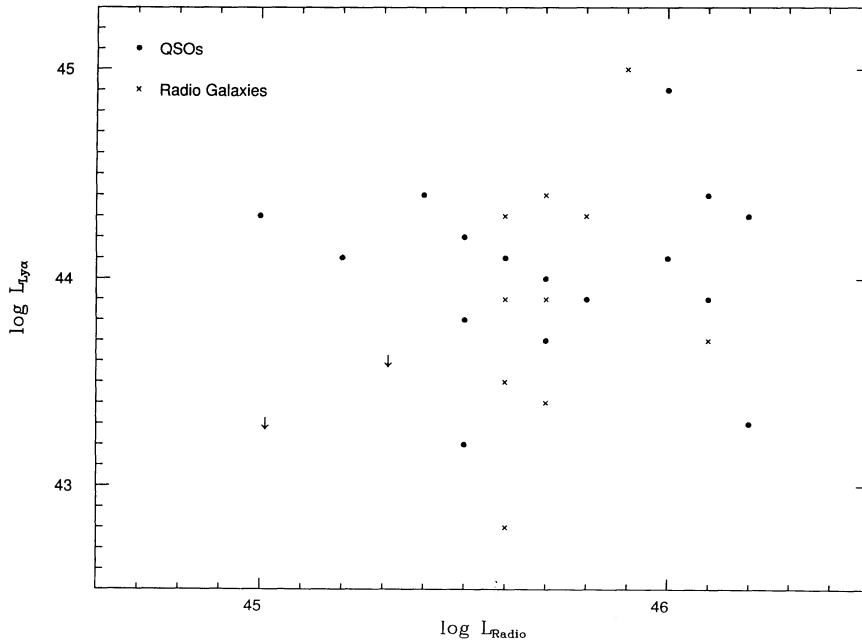


FIG. 3.—The log of the luminosity of the *spatially resolved* Ly α emission (in ergs s^{-1} ; see Table 2) is plotted against the nonthermal radio luminosity ($\equiv 10\lambda P_\lambda$ at $\lambda = 6$ cm, in ergs s^{-1} ; see Table 4) for the QSOs in our sample (filled circles). Similar data for high- z radio galaxies are indicated by crosses and are taken from McCarthy (1988).

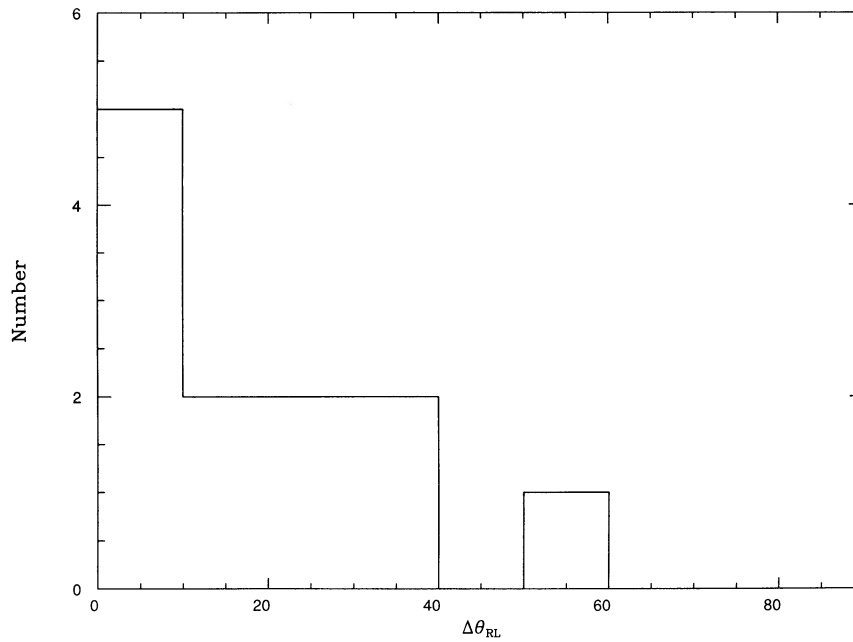


FIG. 4.—A histogram of the difference in the position angle of the radio source and the Ly α nebula (constrained to be $\leq 90^\circ$) for the 12 QSOs for which an unambiguous Ly α position angle can be defined (see Table 4 and the text for details).

which the radio emission is brighter in nine of the 10 cases (the only exception is Q0109+176). In addition, nine of these 10 QSOs with asymmetric Ly α nebulae have detectable radio emission between the nuclear radio source and *one* of the two outer hot spots (Q2150+053 being the only exception). We will call these one-sided features “jets,” but note that better radio maps are needed to confirm this classification in many cases. In eight of these nine QSOs, the Ly α emission is brighter on the radio jet side (Q0109+176 again being the only exception).

McCarthy, van Breugel, & Kapahi (1990) have recently found that high-redshift radio *galaxies* almost always have the brightest optical line emission on the same side as the nearer of the two radio hot spots. We see a possible, but not statistically significant trend in the high- z QSOs: of the seven cases in which we can make a comparison, the Ly α is brighter on the side of the nearer radio hotspot in five cases (see Table 4).

BTT have recently published spectra of 16 of the QSOs in our sample and have identified absorption lines in these spectra. One of the original motivations of our imaging program was to attempt to discover an emission-line counterpart to the gas producing the strong C IV $\lambda 1549$ $z_{\text{abs}} \approx z_{\text{em}}$ absorption-lines often seen in radio-loud QSOs (e.g., Foltz et al. 1988; BTT). Indeed, of the 16 QSOs we have in common with BTT, six meet the Foltz et al. criteria for “strong, associated absorption”: rest-frame equivalent width of the C IV doublet $W_{0,\text{CIV}} > 1.5 \text{ \AA}$ and a rest-frame velocity difference $\Delta v < 5000 \text{ km s}^{-1}$, where $\Delta v \approx c|z_{\text{em}} - z_{\text{abs}}|/(1 + z_{\text{em}})$. Four more have detectable C IV absorption with $1.5 \text{ \AA} > W_{0,\text{CIV}} > 0.5 \text{ \AA}$ and $\Delta v < 5000 \text{ km s}^{-1}$. These statistics are consistent with the results of the Foltz et al. “mini-survey” of 12 high- z 3CR QSOs.

However, while both Ly α nebulae and $z_{\text{abs}} \approx z_{\text{em}}$ systems are common in our QSOs, we find no correlation between the two phenomena. Specifically, none of the following correlate with $W_{0,\text{CIV}}$: the Ly α luminosity of the nebula, the fraction of the

total Ly α luminosity provided by the nebula, the equivalent width of the nebular Ly α , or the total Ly α equivalent width. We will briefly discuss the implications of these results in § IV below.

3.2. Spatially Resolved Continuum Properties

Perhaps our most striking result is the discovery that the continuum emission is spatially resolved in at least six, and probably 10, of 18 high- z QSOs. The PSS continuum images for the spatially resolved QSOs are displayed in Figure 5 and the RSB profiles are compared to the PSFs in Figure 6 for all 18 QSOs (the 19th QSO, Q1345+584, had no stars suitable for determining the PSF in its continuum image). The continuum properties of the QSOs are summarized in Table 3, while details concerning individual QSOs may be found in the Appendix. The general properties of the spatially resolved “fuzz” are as follows:

1. The continuum images are generally dominated by the unresolved QSO proper. The relative fraction of the continuum flux from the fuzz ranges from less than 3% of the total to $\approx 40\%$ in Q0445+097. Other QSOs in which the fuzz is relatively prominent ($\approx 20\%$ of the total flux) include Q0549–213, Q1318+113, and Q2338+042 (note, however, that the broadband image of the fuzz in this last QSO is significantly contaminated at the $\approx 30\%$ level by Ly α emission).

2. The luminosity of the fuzz (measured at a rest wavelength of $\approx 1200 \text{ \AA}$ in the QSO rest frame) typically ranges from one to several $\times 10^{45} \text{ ergs s}^{-1}$. We have calculated this luminosity (L_{fuzz}) by first correcting the U or B magnitude for Ly α emission in the filter bandpass and then for Galactic extinction (Burstein & Heiles 1982), converting this corrected magnitude to an equivalent flux density, computing the monochromatic power P_{λ_0} in the QSO rest frame (where $\lambda_0 \approx 1200 \text{ \AA}$; see Table 3), and then defining $L_{\text{fuzz}} = \lambda_0 P_{\lambda_0}$. Note that this procedure involves no (highly uncertain) K -correction. These fuzz luminosities are quite similar to the total rest-frame UV luminin-

TABLE 4
COMPARISON OF THE RADIO AND OPTICAL PROPERTIES

QSO (1)	$\Delta \log L_{\text{RL}}$ (2)	$\Delta \log D_{\text{RL}}$ (3)	Θ_{R} (4)	Θ_{L} (5)	Θ_{C} (6)	$\Delta\Theta_{\text{RL}}$ (7)	$\Delta\Theta_{\text{RC}}$ (8)	JS? (9)	BS? (10)	NS? (11)
Q0017+154.....	1.9	0.1	144	0a	...	36
Q0109+176.....	2.3	0.7	110	-90a	...	160	...	N	N	N
Q0225-014.....	1.7	0.5	-52	-60b	-60b	8	8
Q0316-203.....	>1.7
Q0445+097.....	1.3	-0.7	-125	-140b	110a	15	125	Y	Y	...
Q0549-213.....	-90	...	-110b	...	20
Q0730+257.....	1.9	-0.1	-41	-45b	-170c	4	?	Y	Y	N
Q0751+298.....	>1.7
Q0758+120.....	1.1	-0.1	-108	c
Q0805+046.....	1.1	-0.5	132	160a	0c	28	?	Y	Y	...
Q0941+261.....	2.2	-0.9	80	80a	...	0	...	Y	Y	...
Q1318+113.....	1.7	-0.3	-151	-160a	85b	9	124	Y	Y	Y
Q1345+584.....	1.0	-0.5	-90	c	Y	Y	Y
Q1354+258.....	0.7	-0.5	-163	170b	70c	27	?
Q1658+575.....	1.5	-0.3	10	r	20c	...	?
Q2150+053.....	2.0	0.2	95	150b	?	55	Y	Y
Q2222+051.....	1.7	-0.5	-143	-145b	...	2	...	Y	Y	Y
Q2251+244.....	>2.9
Q2338+042.....	1.9	-0.6	102	135b	120c	33	?	Y	Y	Y

COL. (2).—The log of the ratio of the luminosity of the nonthermal radio source (estimated to be $\approx 10\lambda P_{\lambda}$ where $\lambda = 6$ cm in the QSO rest frame, taken from Barthel et al. 1988) to the luminosity of the *spatially extended* Ly α emission (see Table 2). The uncertainties in this ratio are dominated by uncertainties in the Ly α luminosities and are given in Table 2. Note that the total emission-line luminosity of the nebulae (summed over all emission lines and corrected for internal extinction) could be significantly larger than our derived $L_{\text{Ly}\alpha}$.

COL. (3).—The log of the ratio of the diameter of the radio source to the diameter of the Ly α nebula. The former parameter is determined from the maps published by Barthel et al. (1988) or (for Q0017+154 only) by Swarup, Sinha, & Saika (1982). The latter parameter is from Table 2, where the uncertainties are also given.

COL. (4).—The position angle (degrees E of N) of the radio source axis. This axis is defined to be along the line joining the fainter to the brighter outer radio hotspots. If the radio source is one-sided, the ratio position angle is taken to be the line joining the nucleus and the outer hotspot.

COL. (5).—The position angle of the Ly α nebula (degrees E of N). Cases denoted by “c” and “r” are too complex or too round (respectively) to assign a position angle. For the other cases, the uncertainties are coded either “a” (uncertain by $<15^\circ$) or “b” (uncertain by 15° – 30°).

COL. (6).—The position angle of the spatially resolved continuum fuzz (degrees E of N). Uncertainties are coded “a” (uncertain by $<15^\circ$), “b” (uncertain by 15° – 30°), or “c” (uncertain by $>30^\circ$).

COL. (7).—The offset in position angle (in degrees) between the principle morphological axis of the radio source and that of the Ly α nebula (see cols. [4] and [5]). The uncertainty in the Ly α position angle dominates the uncertainty in this quantity (see col. [5]).

COL. (8).—The offset in position angle (in degrees) between the principle morphological axis of the radio source and that of the spatially resolved optical continuum (the fuzz). The uncertainty in the fuzz position angle dominates the uncertainty in this quantity (see col. [6]). A value for the radio-optical offset is given only when the uncertainties in the latter are $<30^\circ$ (see col. [6]).

COL. (9).—Is the brighter Ly α emission on the same side of the QSO as the one-sided radio jetlike structure? See text and Appendix for details.

COL. (10).—Is the brighter Ly α emission on the same side of the QSO as the brighter radio emission? See text and Appendix for details.

COL. (11).—Is the brighter Ly α emission on the same side of the QSO as the nearer of the two outer radio hotspots? See text and Appendix for details.

osities of high- z radio galaxies (see Chambers 1989; McCarthy 1988).

3. Typical sizes of the fuzz (measured at isophotal radii of $\approx 1\%$ of the night sky brightness ≈ 27 mag arcsec $^{-2}$) are $5''$ – $9''$ (≈ 40 – 80 kpc). These sizes are similar to the sizes of the QSO Ly α nebulae and of the continuum structures in high- z radio galaxies.

4. While the amount of morphological information is quite limited, the fuzz is often distributed rather asymmetrically about the QSO (see Fig. 5 and the Appendix for details).

5. There is some tendency for the QSOs with the most (least) conspicuous continuum fuzz to also have the most (least) conspicuous Ly α nebulosity. That is, the three QSOs that are unresolved in Ly α (Q0316–203, Q0751+298, and Q2251+244) are all unresolved in the continuum, while the three QSOs with $L_{\text{fuzz}} > 15\% L_{\text{tot}}$ and with Ly α images (Q0445+097, Q1318+113, and Q2338+042) are among the six QSOs with Ly α nebulae that produce more than 25% of the

total Ly α emission. There are exceptions, however: Q0758+120 is unresolved in the continuum but has a spectacular Ly α nebula that produces $\approx 50\%$ of the total Ly α .

6. Somewhat surprisingly, the Ly α nebulae and continuum fuzz are sometimes misaligned (see Table 4). Q0445+097 is the most dramatic and clear-cut example of misaligned Ly α and continuum structures: while the Ly α is most extended along the NNE/SSW axis (and brightest to the SW), the continuum is elongated primarily in the ESE/WNW direction (misaligned with the Ly α by $\sim 70^\circ$). The other QSO with the most clearly misaligned Ly α nebulosity is Q1318+113. Images with higher spatial resolution will be needed to further quantify this, since the fuzz structure is often unclear close to the QSO. We note that this misalignment provides reassuring evidence that spatially resolved Ly α emission transmitted through our continuum filter bandpass is not usually making a significant contribution to the continuum fuzz (see above).

7. In contrast to the situation for high-redshift radio gal-

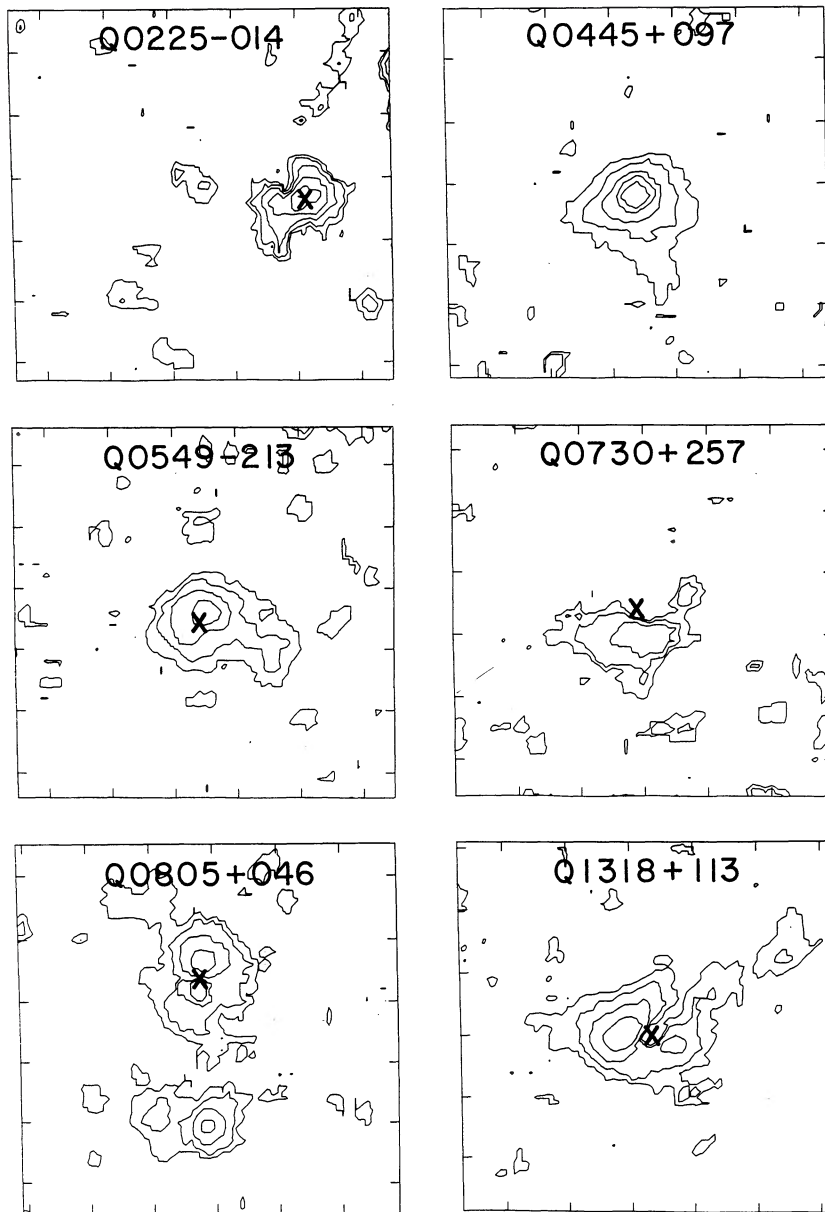


FIG. 5.—Contour plots of the continuum-band images of the nine high- z QSOs with the best-resolved continuum emission (we do not show Q2150+053 which is only very marginally resolved). Except for Q0445+097, the images have had the contribution of the unresolved nuclear point source (the QSO proper) subtracted off at the position marked with a cross, using stars in the same image as a model of the point spread function (these are the PSS images; see § 2.2). Each image is $18'' \times 18''$ in size with north to the top and east to the left. The value of the lowest contour level (in magnitudes arcsec $^{-2}$) is given in Table 5. Each successive contour represents a change of ≈ 0.75 mag (e.g., exactly a factor of 2 in surface brightness). These images have been smoothed with a 4×4 pixel median filter to highlight low-surface-brightness emission and to minimize the effects of cosmic rays and “hot” pixels. Note that the structures visible in Q0805+046 and Q2338+042 are significantly contaminated with Ly α emission (see text).

axes (McCarthy et al. 1987b; Chambers, Miley, & van Breugel 1987), the continuum fuzz does *not* appear to strongly align with the radio source axis (see Table 4). The fuzz in Q0445+097 (the brightest and most easily studied example) is misaligned by nearly 60° with the radio axis. The other best example of a QSO whose continuum fuzz is definitely misaligned with the radio axis is Q1318+113. Further analysis of the degree of misalignment is hampered by uncertainties in the structure of the continuum fuzz in many of the QSOs.

8. Neither the luminosity of the fuzz nor the relative fraction of the total UV continuum luminosity provided by the fuzz

correlates with the presence or strength of $z_{\text{abs}} \approx z_{\text{em}}$ C IV absorption-line systems documented by BTT.

4. DISCUSSION

4.1. Basic Physical Properties of the Ly α Nebulae

The most natural interpretation of the Ly α nebulae is that they are the interstellar or circumgalactic medium of the QSO host (proto?) galaxy and are being photoionized by the QSO. While we can not exclude alternative ionization sources (e.g., the young stars that may produce the UV-continuum fuzz or

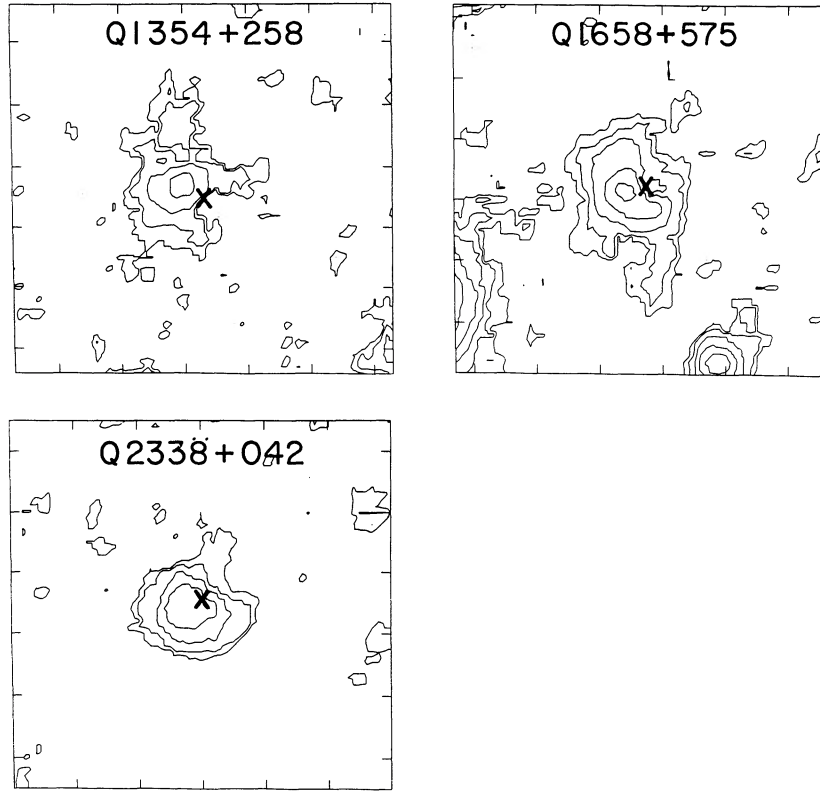


FIG. 5—Continued

the relativistic particles in the radio plasma), the *observed* rest-frame UV continua from the QSOs are typically more than two orders of magnitude more luminous than would be required to “power” the Ly α luminosities of the nebulae. Unless the nebulae are somehow hidden from the QSO, photoionization by the QSO is unavoidable.

Adopting a model in which the nebulae are in photoionization equilibrium with the diffuse QSO radiation field allows us to deduce the approximate physical parameters in the nebulae by following the arguments in (for example) Crawford, Fabian, & Johnstone (1988, hereafter CFJ) and Baum & Heckman (1989a). The electron number density of a photoionized cloud (n_c) located a distance r from an ionizing source with a Lyman continuum luminosity (Q) and characterized by an ionization parameter U (defined as the ratio of ionizing photons to electrons in the cloud) is given by

$$n_c = Q/(4\pi r^2 U c). \quad (1a)$$

Expressing these parameters in convenient units (Q in units of 10^{57} s^{-1} , r in units of $10^{23} \text{ cm} \approx 32 \text{ kpc}$, and U in units of 10^{-3}) gives

$$n_c = 270 Q_{57} r_{23}^{-2} U_{-3}^{-1} \text{ cm}^{-3}. \quad (1b)$$

Our QSO continua (measured at a rest-frame wavelength of $\approx 1200 \text{ \AA}$) imply typical values of $Q \approx 1$ to $4 \times 10^{57} \text{ s}^{-1}$ for a ionizing source with the form $P_\nu \propto \nu^{-1}$. The maximum dimensions of the nebulae are of-order few times 10^{23} cm . Values for U in AGNs are inferred from comparison of the relative strengths of high-ionization and low-ionization lines to photoionization models. Our images then do not directly specify U . However, the values for U that are determined observationally

for AGNs lie in the relatively narrow range between $\approx 10^{-4}$ to $\approx 10^{-2}$ (the basic physics that constrains the clouds to this

TABLE 5
CONTOUR VALUES IN FIGURES 1 AND 5

QSO (1)	Ly α (2)	Continuum (3)
Q0017+154.....	3.6	...
Q0109+176.....	2.4	...
Q0225-014.....	2.5	26.3
Q0445+097.....	2.6	25.6
Q0549-213.....	...	27.2
Q0730+257.....	1.7	27.3
Q0758+120.....	0.9	...
Q0805+042.....	1.1	26.9
Q0941+261.....	1.0	...
Q1318+113.....	2.8	26.3
Q1345+584.....	2.6	...
Q1354+258.....	2.1	27.2
Q1658+578.....	1.1	27.1
Q2150+053.....	2.6	...
Q2222+051.....	1.3	...
Q2338+042.....	1.5	27.3

COL. (2).—The Ly α surface brightness of the lowest contour in Fig. 1 in units of $10^{-17} \text{ ergs cm}^{-2} \text{ s}^{-1} \text{ arcsec}^{-2}$ above the Earth's atmosphere. Each successive contour in Fig. 1 represents an increase in surface brightness by a factor of 2.

COL. (3).—The surface brightness of the lowest contour in Fig. 5 in units of U or B magnitudes arcsec^{-2} above the Earth's atmosphere. Each successive contour in Figure 5 represents an increase in surface brightness by a factor of 2 ($\approx 0.75 \text{ mag}$).

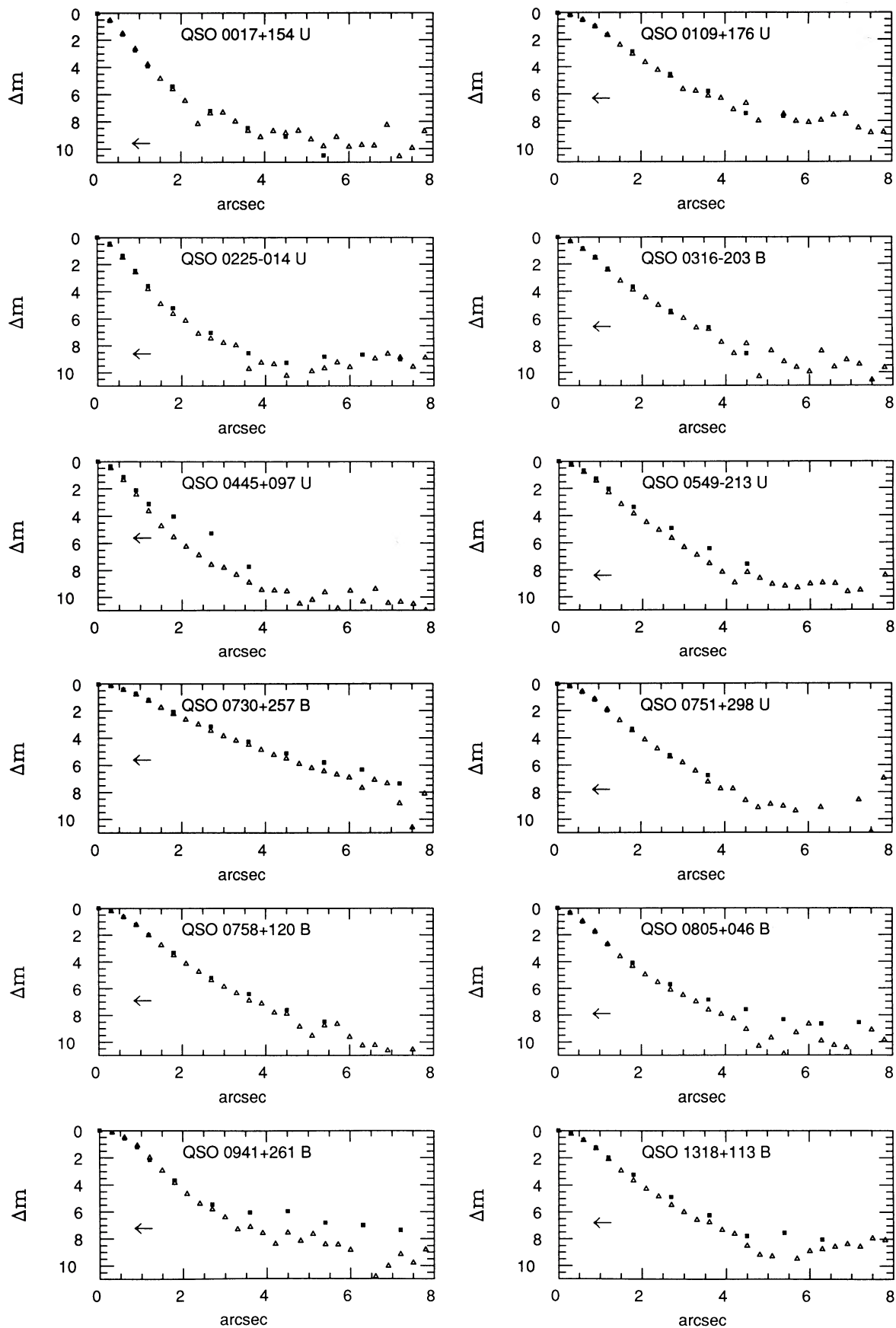


FIG. 6.—Comparison of the azimuthally averaged radial surface brightness profiles (RSBPs) of our sample of 18 QSOs (*filled squares*) and the point spread functions (PSFs) as measured with bright stars (*open triangles*) in the broad-band UV continuum images. The surface brightnesses are given in magnitudes relative to the brightest central pixel. The RSBPs are reliable down to a level of $\approx 1\%$ of the sky brightness (level indicated by a horizontal arrow in each plot). Note that in no case is the PSF broader than the RSBP, while the reverse is true in 10 of the 18 QSOs.

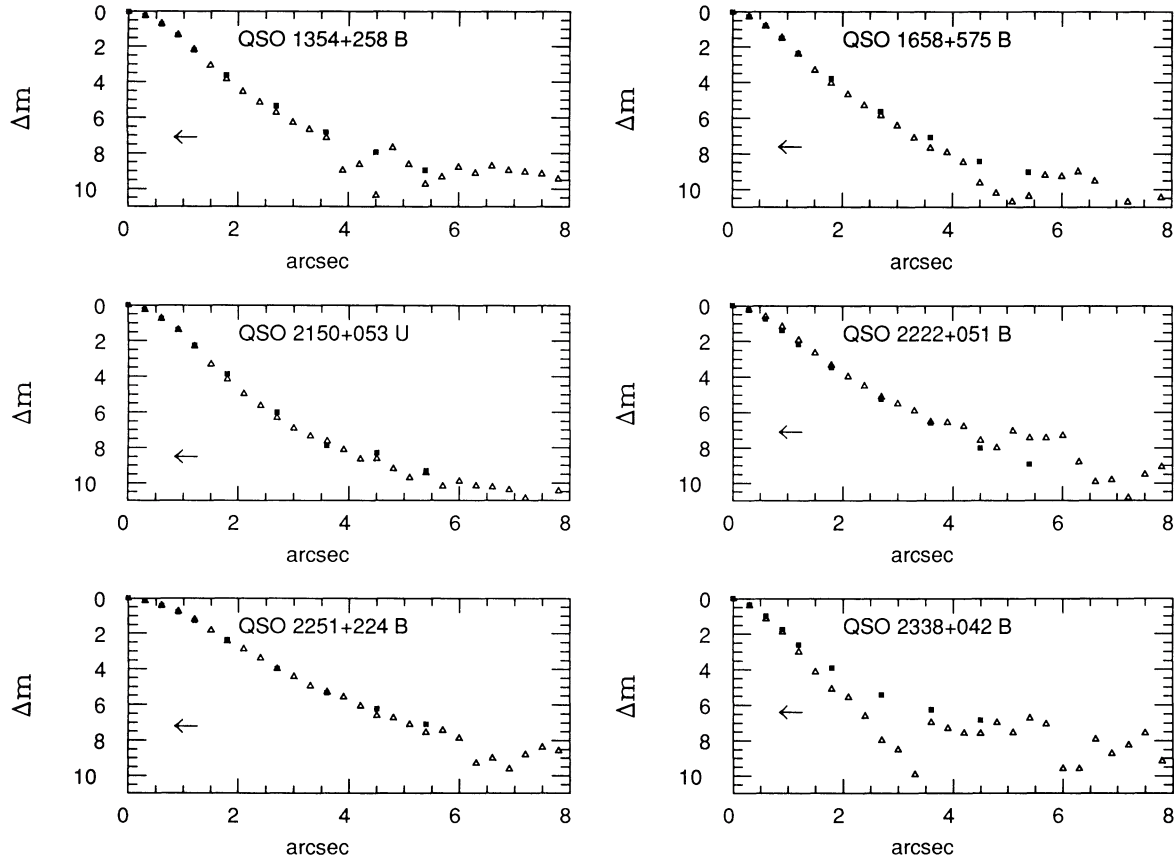


FIG. 6—Continued

range is discussed in Krolik, McKee, & Tarter 1981). More particularly, CFJ and CF have determined that $\log U \approx -2.5 \pm 0.5$ in the nebulae surrounding radio-loud QSOs at $z < 1$. This is similar to the typical values inferred by McCarthy (1988) and Robinson et al. (1987) in the nebulae surrounding high- and low-redshift radio galaxies respectively.

We therefore suggest that the typical electron densities of the Ly α clouds in the QSO nebulae range from several tens in the outermost portions of the nebulae (≈ 100 kpc) to several thousand at the innermost portions (≈ 10 kpc). The implied pressures ($P \approx 2n_e kT$) are then of-order 10^{-10} to 10^{-8} dyne cm^{-2} .

Adopting these densities we can then estimate the mass and the volume filling factor for the emission-line gas in our high- z QSO nebulae. We adopt a King-type density law given by $n_c(r) = n_{c,0} [1 + (r/r_c)^2]^{-1}$ with r_c smaller than our seeing disk, i.e. similar to the density profiles inferred for the X-ray gas in early-type galaxies (see Sarazin 1986) and implying that U is constant with radius outside the core. Assuming case B recombination, it is then straightforward to show that the total cloud mass is related to the Ly α luminosity by

$$M_c = [L_{\text{Ly}\alpha} \mu / (\epsilon_{\text{Ly}\alpha} n_c)] * (r_{\min} r_{\max} / r_0^2), \quad (2a)$$

where μ is the mean mass per particle, $\epsilon_{\text{Ly}\alpha}$ is the standard case B value for the Ly α emissivity ($\approx 3 \times 10^{-24}$ ergs $\text{cm}^3 \text{s}^{-1}$; see Osterbrock 1989), and r_{\min} and r_{\max} are the innermost and outermost radii of the nebula, respectively. To evaluate this expression, we take n_c to be measured at $r_0 \equiv (r_{\min} r_{\max})^{1/2}$. We can then rewrite equation (2a) in convenient units as

$$M_c = 3 \times 10^8 L_{\text{Ly}\alpha,44} (n_c/100) M_\odot, \quad (2b)$$

or combining this with equation (1b), we get

$$M_c = 3 \times 10^7 L_{\text{Ly}\alpha,44} Q_{57}^{-1} U_{-3} M_\odot. \quad (2c)$$

We therefore estimate that the mass of the Ly α -emitting clouds in a typical high- z QSO nebula is of-order $10^8 M_\odot$.

The modest masses and large densities of the Ly α clouds imply that they occupy only a very small fraction of the volume of the nebula. This volume filling factor is given by

$$ff = 1.3 \times 10^{-8} L_{\text{Ly}\alpha,44} U_{-3}^2 Q_{57}^{-2} (r_{\min}/10 \text{ kpc}). \quad (3)$$

The observed Ly α luminosities of the nebulae compared to the estimated luminosities of the ionizing continuum imply that the clouds intercept only $\sim 0.5\%$ (on-average) of the Lyman continuum radiation from the QSO. The clouds then have a covering factor $\geq 0.5\%$ (where the equality applies if the clouds are optically thick to the Lyman continuum radiation).

Elementary considerations of ionization equilibrium imply that the thickness of the ionized skin of a cloud irradiated by a QSO will be

$$l_{\text{HII}} \approx 10^{20} U_{-3} n_c^{-1} \text{ cm} \approx 4 \times 10^{17} Q_{57}^{-1} r_{23}^2 U_{-3}^2 \text{ cm}. \quad (4)$$

Thus for typical values of U and Q , the ionized portion of an individual cloud can be no larger than $\approx 10^{17}$ cm thick in the inner nebula and $\approx 10^{19}$ cm thick in the outer.

4.2. Cloud Confinement and the Intracloud Medium

As CFJ and CF have argued, unless the Ly α emitting material is confined, it will dissipate on very short time scales

(maximum lifetime \approx few times 10^4 yr for a 10^{18} cm thick photoionized region expanding at its sound speed of ≈ 10 km s^{-1}). In order that an unconfined cloud be long-lived, it must be physically large and hence very optically thick to ionizing radiation. It will then be slowly losing mass via photoevaporation from a thin ionized skin on the side of the cloud facing the QSO. An instantaneous mass of $\approx 10^8 M_\odot$ in the Ly α -emitting material (see above) being photoevaporated every few times 10^4 yr, implies a loss rate of several thousand M_\odot per year of H II from the clouds. Over the radio source lifetime ($\approx 10^8$ yr), a total of several times $10^{11} M_\odot$ will be photoevaporated by the QSO.

CFJ and CJ argue that such large gas masses in dense clouds are implausible, and therefore contend that the clouds are likely to be in pressure balance with a hot intercloud medium (ICM). The temperature of this ICM is expected to be of-order 10^7 K, since this is close to both the equilibrium temperature for a medium that is Compton-heated (or cooled) by a QSO and the Virial temperature in the potential of a massive galaxy (see Rees 1988; Krolik, McKee, & Tarter 1981; Krolik & Kallman 1988; Mathews & Ferland 1987). We can then calculate the mass of an ICM with a temperature $T_{IC,7}$ (in units of 10^7 K) that is in pressure-balance with the emission-line clouds (assumed to have $T \approx 10^4$ K, as set by photoionization):

$$M_{IC} = 4 \times 10^{12} Q_{57} (r_{max}/50 \text{ kpc}) U_{-3}^{-1} T_{IC,7}^{-1} M_\odot. \quad (5)$$

Taking $Q_{57} \approx 2$, $U_{-3} \approx 3$, $r_{max} \approx 50$ kpc, and $T_{IC,7} \approx 1$ implies that $M_{IC} \approx$ few times $10^{12} M_\odot$ —somewhat in excess of the mass of the stellar population in a giant elliptical galaxy.

Could this hypothetical ICM be detected as a thermal X-ray source? For the density law given in equation (1), and the expression for the total bremsstrahlung emissivity in Tucker (1977) we get

$$L_x(\text{tot}) \approx 5 \times 10^{46} Q_{57}^2 U_{-3}^{-2} T_{IC,7}^{-1.5} (r_c/5 \text{ kpc})^{-1} \text{ ergs s}^{-1}. \quad (6)$$

Taking our best estimates for Q , U , and T_{IC} (see above) we find that $L_x(\text{tot}) \approx 2 \times 10^{46} (r_c/5 \text{ kpc})^{-1} \text{ ergs s}^{-1}$. An independent estimate of L_x comes from comparing our estimated pressures in the QSO nebulae to those at the same radii in well-studied local examples of X-ray luminous giant ellipticals. Comparing the radial pressure profiles for M87 and MKW 3's given in CF to the pressures implied by equation (1), and assuming that $L_x \propto P^2$, we again find that the estimated X-ray luminosity of the ICM in our high- z QSOs is $\approx 10^{46} \text{ ergs s}^{-1}$ (integrated between 0.5 and 4.5 keV in the QSO rest frame).

The only QSO in our sample known to us to have a published X-ray luminosity is 3C 9 (Q0017+154), measured by Zamorani et al. (1981) to have $L_x = 4 \times 10^{45} \text{ ergs s}^{-1}$ (between 0.5 and 4.5 keV in the QSO rest frame). Assuming our other QSOs are similar to radio-loud QSOs in general (see Zamorani et al. 1981), the observed continuum luminosities at 1200 Å (see Table 3), imply that our QSOs have typical X-ray luminosities of $\approx 10^{46} \text{ ergs s}^{-1}$. It is generally believed that the X-ray continuum in highly luminous AGNs is produced by the central engine, but there is little direct evidence that this is the case in high- z QSOs. The similarity between our predicted luminosity of the ICM and the observed X-ray luminosity of 3C 9 raises the possibility that the ICM might make a significant contribution to the observed X-rays. Hence, observations with high spatial resolution (≈ 1 arcsecond) are required to determine what fraction of the observed X-rays arise in the QSO proper versus the ICM. Could the additional X-ray emission from the ICM help explain why radio-loud QSOs are significantly

stronger X-ray emitters than radio-quiet QSOs of comparable optical luminosity (e.g., Zamorani et al. 1981)?

Begelman & Cioffi (1989) and Chambers (1989) have recently discussed Scheuer's (1974) contention that the bulk of the energy carried by a powerful radio jet is used to inflate a "cocoon" around the radio source. This cocoon consists of an inner region of shocked jet fluid, surrounded by shocked circumgalactic (halo) gas. Such a cocoon is an attractive possibility for the ICM in the QSO Ly α nebulae. Given the characteristic pressures we deduce and sizes we measure for the Ly α nebulae, the total energy content of the cocoon would have to be $\approx 10^{61}$ ergs (similar to the total radio synchrotron energy budget for a typical observed radio luminosity of several times $10^{45} \text{ ergs s}^{-1}$ and an estimated radio lifetime of $\approx 10^8$ years). More quantitatively, Begelman & Cioffi (1989) derive a characteristic cocoon pressure of

$$P_c \approx 2 \times 10^{-9} L_{j,46}^{1/2} \beta_j^{1/2} A_{h,44}^{1/2} A_{c,46}^{-1} n_{a,-2}^{1/2} \text{ dyn cm}^{-2} \quad (7)$$

for a cocoon of cross-sectional area (transverse to the jet axis) of A_c (in units of 10^{46} cm^2) inflated by a jet that carries kinetic energy outward at a rate L_j (in units of $10^{46} \text{ ergs s}^{-1}$) with a velocity β_j (in units of c) into an ambient medium with number density n_a (in units of 10^{-2} cm^{-3}), and where the jet kinetic energy is "thermalized" in a radio hotspot of cross-sectional area A_h (in units of 10^{44} cm^2). Thus, for reasonable values for the parameters in equation (7), we find a cocoon pressure that is similar to the inferred pressures in the Ly α clouds.

While this is encouraging, one possible problem with a cocoon model is that there are many cases of Ly α nebulae that extend well beyond the outer radio "hotspots" (e.g., by a factor of 8 in Q0941+261 and a factor of 5 in Q0445+097). It is possible that radio maps with greater sensitivity and dynamic range might show that the radio plasma is comparable in extent to the Ly α nebula. For example, a large cocoon might have been created at some earlier stage when the radio source was significantly larger than at present. It is also possible that the cases in which the Ly α emission extends well beyond the radio source are QSOs in which the radio sources are highly foreshortened (viewed approximately end-on). Since the cocoons are theorized to be much more spheroidal than the radio sources, the projected size of the cocoon will be relatively insensitive to these viewing angle effects, and the foreshortened cocoon could appear significantly larger than the foreshortened radio source.

Finally, we consider the possibility that the Ly α clouds are confined by the ram pressure of an outflowing wind (e.g., Ikeuchi 1981; Heckman, Armus, & Miley 1990). For a balance between cloud pressure and wind ram pressure, equation (1b) then implies that the total momentum flux in a wind flowing out into a solid angle of Ω steradians must be

$$dp/dt \approx 10^{38} Q_{57} U_{-3}^{-1} \Omega/4\pi \text{ dynes}. \quad (8a)$$

Taking a wind velocity of v_4 in units of 10^4 km s^{-1} , the corresponding mass and kinetic energy outflow rates in the wind are then

$$dM/dt \approx 1500 Q_{57} U_{-3}^{-1} v_4^{-1} \Omega/4\pi M_\odot \text{ yr}^{-1}, \quad (8b)$$

$$dE/dt \approx 5 \times 10^{46} Q_{57} U_{-3}^{-1} v_4 \Omega/4\pi \text{ ergs s}^{-1}. \quad (8c)$$

Thus, a wind that is potent enough to confine the clouds must have a mechanical luminosity comparable to the UV luminosity of the QSO (see Table 3). For a radio source lifetime of $\approx 10^8$ yr, the total mass lost in the wind is $\approx 10^{11} M_\odot$ and the total mechanical energy output is $\approx 10^{62}$ ergs.

4.3. Relationship to the Radio Source

As discussed in § 3 above, there is clear morphological evidence for a relationship between the thermal gas ($\text{Ly}\alpha$ nebulae) and the relativistic plasma (the radio source) in our sample of high- z QSOs: the $\text{Ly}\alpha$ nebulae and radio sources are preferentially aligned with one-another to within $\approx 30^\circ$ and the $\text{Ly}\alpha$ emission is preferentially extended on the same side as the brighter radio emission (which often has a jetlike morphology).

The most plausible interpretation of the alignment effect is that the gas is photoionized by radiation that escapes the QSO anisotropically along the radio jet axis. There is a growing body of evidence that “radiation cones” aligned with radio axes are common in many classes of AGNs (see Miller 1989 and many papers in the volume edited by Meurs & Fosbury 1990). Alternative alignment schemes in which the radio plasma is directly involved in heating the $\text{Ly}\alpha$ nebula (via shocks, relativistic particles, or *in situ* UV synchrotron radiation) are less attractive because there are many cases in which the $\text{Ly}\alpha$ emission extends factors of several times further from the QSO than the radio plasma. Moreover, as noted above, the QSO continuum is more than adequate energetically to ionize the gas.

The shared radio- $\text{Ly}\alpha$ asymmetry can be plausibly interpreted in at least two ways. First, it is possible that both the radio and $\text{Ly}\alpha$ emission are *intrinsically* symmetric (two-sided). The radio emission then appears one-sided or asymmetric because of the relativistic “Doppler boosting” of the approaching side, while the $\text{Ly}\alpha$ nebula appears asymmetric because of heavier dust extinction suffered by the back side of the nebula.

The destruction of $\text{Ly}\alpha$ photons via resonant scattering and dust absorption requires very little dust to be present because of the large path-length the $\text{Ly}\alpha$ photons must traverse as they attempt to random-walk out of the nebula (e.g., Adams 1975). Fall, Pei, & McMahon (1989) have derived a critical H I column density for the quenching of $\text{Ly}\alpha$ emission given by

$$N_{\text{HI crit}} \approx 9 \times 10^{19} (k/k_{\text{MW}})^{-3/4} (\sigma/100)^{1/2} \text{ cm}^{-2}, \quad (9a)$$

where k and k_{MW} are the dust-to-gas ratios in the H I within the QSO nebula and the Milky Way, respectively, and σ is the velocity dispersion in the H I gas in the QSO nebula in km s^{-1} . The H I mass implied by this column density is

$$M_{\text{HI crit}} \approx 6 \times 10^9 (k/k_{\text{MW}})^{-3/4} (\sigma/100)^{1/2} (D_{\text{HI}}/100 \text{ kpc})^2 M_{\odot}, \quad (9b)$$

where D_{HI} is the diameter of the H I nebula. This mass is quite reasonable even compared to present-day massive spiral galaxies. H I could survive in the environment of the QSO only if it were shielded from the ionizing radiation of the QSO. For example, in the “ionization cone” model for QSOs, the H I could be confined to the region perpendicular to the radio axis. If the $\text{Ly}\alpha$ asymmetry does arise via resonant scattering with dust, the nebulae should be far more symmetric when imaged with emission-lines like $[\text{O II}] \lambda 3727$, $[\text{O III}] \lambda 5007$, or $\text{H}\alpha$. Thus, near-IR observations of the QSO nebulae can directly test this idea.

Alternatively, it is possible that the nebulae and the radio sources are *intrinsically* asymmetric. Blandford & Konigl (1979) and others have argued theoretically that the interaction between a radio jet and dense ambient clouds can give rise to intense radio synchrotron emission (see van Breugel et al. 1985

for observational support for this idea). Thus, if the gas were asymmetrically distributed about the QSO, the asymmetric radio emission might be caused by the more intense interaction between the radio and thermal plasmas on the side where the gas is most abundant. Indeed, McCarthy, van Breugel, & Kapahi (1990) have shown that there is a one-to-one correspondence between the side on which the emission-line gas is in radio *galaxies* is brighter and the side on which the radio hot spot is closer to the nucleus. This favors an intrinsic origin for radio/emission-line asymmetries in radio galaxies (see also Pedelty et al. 1989a, b).

It is quite plausible that the gas will have an asymmetric distribution around a high- z QSO. The most robust argument is a simple time scale one: the orbital time for gas in a galaxy potential at a radius of ≈ 30 kpc ($\approx 10^9$ yr) is comparable to the age of the universe at $z \approx 2-3$, and thus such a large structure may not yet have had time to relax into a symmetric configuration (see Rees 1988). More speculatively, Carlberg (1990) has argued that the cosmic evolution of the QSO population is driven by the evolution of the galaxy merger rate. If high- z QSOs are preferentially associated with galaxy interactions (as appears to be the case for powerful AGNs at low redshifts; see, e.g., Heckman 1990 and references therein) this would provide a simple physical explanation for large-scale asymmetric gas distributions around the QSOs.

One argument against this “intrinsically one-sided” model for the shared radio- $\text{Ly}\alpha$ asymmetry is the discovery by Laing (1988), Garrington et al. (1988), and Garrington, Conway, & Leahy (1990) that the radio emission on the side of the bright radio jet in radio-loud QSOs is less Faraday depolarized than the emission on the other side. If the depolarization asymmetry were due to the presence of more thermal plasma on the more strongly depolarized side, then the $\text{Ly}\alpha$ should be stronger on this side. This is just the opposite to the effect we observe. The Laing-Garrington result is readily explained by the Doppler-boosting-plus-dust model for the shared $\text{Ly}\alpha$ /radio asymmetry: since the radio-jet side is the near side of the radio source, it is hence viewed through less of a depolarizing circumgalactic medium than the emission from the back side. Unfortunately, we have only three QSOs in common with the Garrington, Conway, & Leahy (1990) sample, and two of these (Q0017+154 and Q0225-014) do not have asymmetric $\text{Ly}\alpha$ nebulae. The third QSO (Q1318+113) has $\text{Ly}\alpha$ on the less depolarized, jet side. It is clearly important to expand the sample of high- z QSOs with both $\text{Ly}\alpha$ images and radio depolarization maps.

Finally, it is tempting to suggest that the interaction between the radio plasma and the dense, high-pressure ambient gas in the $\text{Ly}\alpha$ nebulae is directly responsible for the small physical sizes and distorted structures of high- z QSO radio sources (e.g., Wardle & Miley 1974; BM). While alternative interpretations for these properties exist (e.g., jet precession, viewing angle effects caused by strong foreshortening of the radio source, QSOs as “young” radio sources, etc.), these alternatives do not *predict* that high- z QSOs should exist in dense, high-pressure environments. In contrast, both the above papers speculated that the cosmic evolution in the properties of QSO radio sources might be regulated by the evolution of the large-scale gaseous environment of the QSO.

Using equation (1) above we have estimated the pressures that are inferred to exist at a fiducial radius of 10 kpc from the nucleus for a sample of low-to-moderate redshift, radio-loud QSOs (CFJ; CF) and our high-redshift, radio-loud QSOs (Fig.

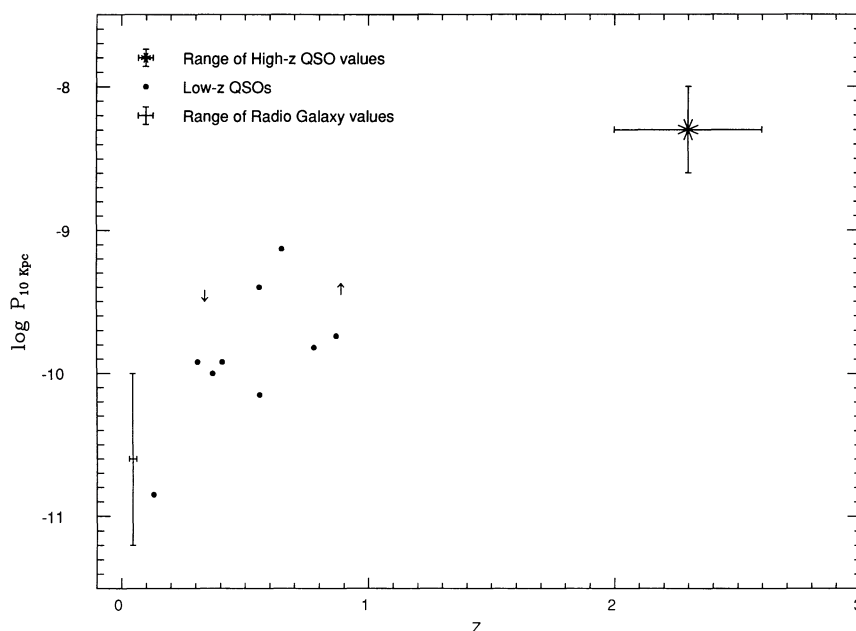


FIG. 7.—Plot of the log of the estimated gas pressure (dyne cm^{-2}) in the emission-line nebulae at a radius of 10 kpc from the nucleus versus redshift for a sample of high-redshift QSOs (large cross at the upper right indicating the range spanned by our QSOs), low-medium redshift QSOs (*open circles*, from CF and CFJ), and low-redshift radio galaxies (Heckman, Baum, & van Breugel 1990; *large cross at lower left*). The pressures for the QSOs assume that photoionization by the QSO with an ionization parameter of $\log U \approx -2.5$ (see text and eq. [1]). The pressures for the radio galaxies are calculated using the densities at radii of several kpc (directly measured with the [S II] $\lambda\lambda 6717, 6731$ doublet) assuming $T \approx 10^4$ K and $P(r) \propto r^{-2}$ between $r \approx$ several kpc and 10 kpc.

7). We have also included the low-redshift ($z < 0.06$) radio galaxies for which Heckman, Baum, & van Breugel (1990) have directly measured the off-nuclear pressures (using spatially resolved measurements of the [S II] $\lambda\lambda 6717, 6731$ line ratio). While Figure 7 implies a huge difference in the gaseous environments of low- and high-redshift radio-loud AGNs, the physical significance of this result is unclear because (apart from the radio galaxies where densities were directly measured) the correlation in Figure 7 is in effect a correlation with Q rather than with z (see equations [1] and [4]). Observations of high-redshift, radio-loud QSOs with significantly smaller Lyman luminosities are needed to disentangle the separate dependences on redshift and Q .

It is intriguing that Garrington & Conway (1990) find that the Faraday depths of the gaseous halos surrounding radio galaxies and radio-loud QSOs increase steadily with redshift (from $\approx 10 \text{ cm}^{-3} \mu\text{G pc}$ at low redshift to ≈ 30 times this value at high redshift). If this increase is due primarily to an increase in the electron density (rather than magnetic field strength), the implied difference between the densities at low and high z is rather similar to the differences we infer in Figure 7. If we adopt typical column densities for the ICM of $\approx 10^{23} \text{ cm}^{-2}$ in our high- z QSOs (see below) the measured Faraday depths then imply magnetic field strengths of $\approx 0.01 \mu\text{G}$ in the gaseous halos surrounding the radio sources.

4.4. Relationship to the $z_{\text{abs}} \approx z_{\text{em}}$ Absorption-Line Systems

The controversy as to whether there is indeed an excess of absorption lines near the emission-line redshift in QSO spectra is not yet resolved (see Foltz et al. 1988; Sargent, Steidel, & Boksenberg 1988). We will therefore only briefly discuss the possible relevance of our new data to the $z_{\text{abs}} \approx z_{\text{em}}$ “associated” absorbers.

The most detailed investigation of these “associated”

absorption-line systems remains the analysis of 3C 191 by Williams et al. (1975). Utilizing the diagnostics provided by the density-sensitive ratio of the strengths of the Si II $\lambda\lambda 1260.4, 1264.8$ lines and by the overall ionization state and strength of the absorption, they were able to determine that the absorbing material has a density of $\approx 10^3 \text{ cm}^{-3}$ and (assuming that it was photoionized by the QSO) is located ≈ 10 kpc from the QSO. Such a density at this radius is remarkably similar to our estimates for the Ly α clouds (see eq. [1b] above).

While this suggests a direct physical link between the $z_{\text{abs}} \approx z_{\text{em}}$ systems and the Ly α nebulae, it is puzzling that we find no statistical evidence for a correlation between these two phenomena (see § 3.1 above). Moreover, the model of Williams et al. predicts far stronger emission from the absorbing material than we actually observe from the nebulae. The predicted rest-frame equivalent width (with respect to the QSO continuum) of the Ly α emission from the absorbing material is $\approx 1200 \text{ \AA}$ for a covering factor of unity. It is hard to reconcile this model with the observed rest-frame equivalent widths of $\approx 10 \text{ \AA}$ or less for the Ly α emission arising in the nebulosity. If this reflects a small covering factor for the absorbing material in our QSOs ($\approx 1\%$), it is then difficult to understand why 25% of the QSOs we have in common with BTT show “associated” absorption with a strength similar to that in 3C 191 ($W_{0,\text{CIV}} > 3 \text{ \AA}$).

It is possible that 3C 191 is not typical of the QSOs in our sample. The Faraday depth of the magneto-ionic material associated with 3C 191 is more than an order-of-magnitude larger than in any of the other ≈ 50 radio sources investigated by Garrington, Conway, & Leahy (1990). Moreover, the $z_{\text{abs}} \approx z_{\text{em}}$ systems associated with the other QSOs in our sample are not known to have Si II $\lambda 1264.8$ absorption, and so could arise in gas of much smaller density located much further from (and not necessarily ionized by) the QSO. In this case, they could produce negligible Ly α emission immediately around the QSO.

However, if 3C 191 is typical, then most of the *total* Ly α emission we observe (e.g., including the very luminous, spatially unresolved emission from the “broad-line region” [BLR]) must also be produced by the $z_{\text{abs}} \approx z_{\text{em}}$ absorbing material. In this case (as Williams et al. pointed out) the BLR in radio-loud high-redshift QSOs is radically different from conventional models of the BLR (e.g., Osterbrock & Mathews 1986): it has a size of ≈ 10 kpc (vs. ≤ 1 pc in the models) and a density of $\approx 10^3 \text{ cm}^{-3}$ (vs. $\approx 10^9 \text{ cm}^{-3}$ in the models). This could be tested by near-IR spectroscopy to search for strong, very broad forbidden-line emission (e.g., [O II] $\lambda 3727$ in the $1.2 \mu\text{m}$ window or [O III] $\lambda 5007$ in the $1.6 \mu\text{m}$ window).

4.5. The Nature of the UV Continuum “Fuzz”

Given the limited amount of information provided by our present data, it is inappropriate to discuss at length the nature of the UV continuum fuzz that surrounds many of the QSOs in our sample. In principle, this could be starlight from a foreground galaxy that may be acting as a gravitational lens on the QSO (e.g., Le Fevre & Hammer 1988 and references therein), QSO light scattering off dust or electrons associated with the Ly α nebulae (see, e.g., Fabian 1989; di Serego Alighieri et al. 1988), or starlight from the QSO host galaxy. Given the many similarities between our high- z QSOs and high- z radio galaxies, it seems likely that the UV continuum fuzz has the same origin in the two classes of objects (indeed, Lehnert et al. 1990b show that the spectral energy distribution of the fuzz in Q0445+097 has the same form as that of the high- z radio galaxies studied by Chambers & Charlot 1990). There is now considerable data concerning the radio galaxies, and the bulk of these data favor the hypothesis that most of the UV continuum emission is produced by young stars in the host galaxy (see Chambers 1989; Chambers & McCarthy 1990; Chambers & Charlot 1990; Lilly 1989). Nevertheless, we will briefly consider both the foreground galaxy/gravitational lens and scattering hypotheses.

As a test of the foreground galaxy hypothesis, we have searched for any correlation between the presence or strength of the UV fuzz and the presence or strength of foreground Mg II $\lambda\lambda 2796, 2803$ absorption (using the data in BTT). We find no such relation, even though Q0445+097 has both the brightest fuzz and the strongest intervening Mg II absorption.

The electron scattering model of Fabian (1989) is particularly relevant if (as we have argued above) a dense, hot ICM may be present around the QSOs. Indeed, equation (1b) can be integrated over radius to yield the column density of electrons in a volume-filling ICM in pressure balance with the Ly α clouds. Expressing this in terms of the Thompson cross section gives an effective optical depth to electron scattering of

$$\tau_{\text{es}} \approx N_e \sigma_T \approx 0.1 Q_{57} U_{-3}^{-1} T_{\text{IC},7}^{-1} (r_c/5 \text{ kpc})^{-1}. \quad (10)$$

Since the typical UV “fuzz” luminosities are $\sim 10\%$ of the QSO luminosities (see Table 3), it is possible that electron scattering plays an important role. However, within the context of the popular “beaming” models, it is strange that the UV fuzz is sometimes strongly misaligned with both the Ly α nebula and radio source: if the Ly α morphology is set by anisotropic escape of ionizing QSO radiation along the radio axis, why would electron-scattered QSO UV continuum light be seen along a very different position angle?

We believe it is most likely that the UV fuzz surrounding our QSOs is indeed starlight from the QSO host galaxy. The enormous UV luminosity of the fuzz ($\approx 2 \times 10^{45}$ ergs s^{-1} on-

average) then implies a huge population of hot stars. Specifically, we find that Kennicutt’s (1983) calculations for steady state star-formation with a Salpeter-like IMF, together with our measured UV fuzz luminosities imply typical star-formation rates of $\approx 100 M_\odot \text{ yr}^{-1}$ for high-mass stars ($M = 10\text{--}100 M_\odot$) and $\approx 600 M_\odot \text{ yr}^{-1}$ for all stars ($0.1\text{--}100 M_\odot$).

While the overall sizes and luminosities of the UV fuzz associated with the high- z QSOs are quite similar to those of the high- z radio galaxies, the QSO fuzz does not appear to be strongly aligned with the radio axis, as is the case with the radio galaxies. We do not wish to overemphasize this result, because (owing to difficulties in accurately subtracting the bright, unresolved light for the QSO proper) the actual structure of the fuzz is often unclear. However, at least two of the four QSOs with the best-resolved fuzz (Q0445+097 and Q1318+113) are *clearly* misaligned with the radio axis.

The apparent lack of a strong alignment of the UV and radio continuum axes in the QSOs might mean that radio-loud QSOs and radio galaxies are closely related, but intrinsically different phenomena. It is also possible (as Barthel 1989 has suggested) that the two classes are intrinsically the same, but are viewed either along (QSO) or perpendicular to (radio galaxy) the axis of the radio jet. In the QSOs, the radio source and UV fuzz would be prolate structures viewed close to their long axes. Because the observed alignment between the radio source and UV fuzz is not perfect in the radio galaxies (typical misalignment angle $\approx 20^\circ$), the foreshortening suffered by the extended radio and UV structures when viewed on-axis in the case of the QSOs may be severe enough to “scramble” the alignment effect. Note that it is just such an effect that Barthel invokes to explain the fact that the QSO radio sources appear smaller and more strongly “bent” than the radio galaxy sources. It is curious, however, that the Ly α is still aligned with the radio source in the QSOs. In the Barthel scheme this can only mean that the intrinsic alignment between the gas and radio source is much better than between the continuum and the radio source (and so is not completely “scrambled” by the foreshortening). Such a better gas-radio alignment is not obvious in the alignment histograms presented in McCarthy et al. (1987a). Further, more quantitative, comparisons of the radio galaxy and QSO radio, Ly α , and continuum images are required.

5. CONCLUSIONS AND IMPLICATIONS

5.1. Summary

We have presented and discussed deep CCD images of 19 high-redshift ($z \approx 2\text{--}3$) radio-loud QSOs obtained with the KPNO 4 m telescope. While several examples of probable companion galaxies near high- z QSOs have been previously detected (e.g., Djorgovski et al. 1987; Hu et al. 1990), our images represent the first large body of quantitative measurements of spatially resolvable structure surrounding high-redshift QSOs at other than radio wavelengths.

The Ly α emission is spatially resolved in 15 of the 18 QSOs with narrow-band images. Each Ly α structure consists of a bright, unresolved core (the QSO proper) and faint nebulousity. These latter have typical diameters of ≈ 100 kpc (at a few times 10^{-17} ergs $\text{cm}^{-2} \text{ s}^{-1} \text{ arcsec}^{-2}$ in the Earth’s frame, or ≈ 100 times brighter in the QSO rest frame). The Ly α luminosity of this resolved structure is typically $\approx 10^{44}$ ergs s^{-1} ($\approx 10\%$ of the total Ly α luminosity). The Ly α nebulae are often asymmetric, but some are symmetric ovals and others are multi-

filamented complexes. The sizes, luminosities, and general morphological characteristics of these nebulae are similar to those of the nebulae associated with radio galaxies with comparable redshifts and radio powers.

We find a clear morphological relationship between the gas and the nonthermal radio source: the radio and Ly α morphological axes typically align to better than $\approx 30^\circ$ and the Ly α is almost always brighter on the same side as the brighter radio emission and/or the one-sided radio jetlike feature. However, the Ly α and radio plasmas are not morphologically related in a detailed sense, nor are their sizes correlated (the Ly α isophotal diameters range from several times smaller to several times larger than the radio source sizes). It is interesting, though, that the three QSOs without detectable Ly α nebulae are the only three QSOs with subarcsecond radio sources. The QSO nebulae lie at the upper end of the broad correlation between radio power and emission-line luminosity defined by radio galaxies.

The most plausible ionization source for the gas is the UV continuum of the QSO. The alignment between the radio and Ly α axes then implies either that dense gas exists preferentially along the radio axis or (more likely) that the ionizing radiation from the QSO escapes anisotropically in broad cones along the radio axis. The physical mechanism producing the correlation between the Ly α and radio "sidedness" is unclear. Differential extinction by dust that obscures the back side of the Ly α nebula, coupled with relativistic "Doppler boosting" of the approaching radio plasma is one possibility. It is also possible that the gas is asymmetrically distributed, with stronger radio emission arising on the side where the more intense interaction between the radio jet and the ambient medium is occurring.

Under the assumption that the nebulae are photoionized by the QSO, we show that they must consist of small (subparsec scale), relatively dense ($n \approx 10^2\text{--}10^3\text{ cm}^{-3}$) clumps with a very small volume filling factor ($\approx 10^{-7}$). The total mass of the Ly α -emitting material is estimated to be of-order $10^8 M_\odot$. If the Ly α clouds are not confined, they must be replenished at a rate of several thousand $M_\odot\text{ yr}^{-1}$ (requiring a total mass of several times $10^{11} M_\odot$ replenished over the radio source lifetime). If the Ly α clouds are in pressure-balance with a volume-filling hot phase at the virial or Compton temperature (see, e.g., Crawford, Fabian, & Johnstone 1988), the mass of the latter will be of order $10^{12} M_\odot$ (comparable to the baryonic mass of a giant elliptical galaxy). It is also possible that the clouds are confined by a high-pressure "cocoon" created by the radio source (e.g., Begelman & Cioffi 1989), or by an thermal wind driven by the QSO (e.g., Ikeuchi 1981). In all cases, a substantial total gas mass ($> 10^{11} M_\odot$) is implied. The overall properties of the nebulae are consistent with the theoretical picture of a young/proto galaxy whose two-phase circumgalactic medium fuels and is then photoionized by, the QSO (e.g., Rees 1988).

It is unclear whether the Ly α nebulae are related to the $z_{\text{abs}} \approx z_{\text{em}}$ "associated" absorption-line systems. While the physical properties of Ly α emission-line clouds in our QSOs and the absorbing material in the well-studied QSO 3C 191 are remarkably similar, we find no evidence for any correlation between the presence or strength of the two phenomena. Moreover, if the $z_{\text{abs}} \approx z_{\text{em}}$ system in 3C 191 is typical of the superficially similar systems in our QSOs, then most of the total Ly α emission from our QSOs (including the BLR) must actually be produced by the absorbing material ($n \approx 10^3\text{ cm}^{-3}$, $r \approx 10$ kpc). This is seriously at odds with our understanding of the BLR in low-redshift AGNs.

We also find that the rest-frame UV continuum can be spatially resolved in at least six, and probably 10 of the 18 QSOs with well-determined point-spread functions. Typical sizes (at $\approx 1\%$ of sky ≈ 27 mag arcsec $^{-2}$) of the "fuzz" are $5''\text{--}9'' \approx 40\text{--}80$ kpc. This component accounts for nearly 40% of the total UV continuum in PKS 0445+097, but only $\approx 3\%\text{--}18\%$ in the other nine cases. The integrated U or B apparent magnitudes of this fuzz are typically $\approx 22 \pm 1$ mag, implying UV continuum luminosities ($\lambda_0 P_{\lambda_0}$ at $\lambda_0 \approx 1200$ Å in the QSO rest frame) of one-to-several times 10^{45} ergs s $^{-1}$. These UV luminosities are similar to those of high-redshift radio galaxies. In contrast to the high- z radio galaxies, the structure of the continuum-emitting fuzz in the QSOs does not appear to be strongly aligned with either the Ly α or the radio emission. At present, we have insufficient data to determine whether the spatially extended UV continuum represents the young stellar population of the host galaxy of the QSO, scattered QSO light, or starlight from a foreground galaxy acting as a gravitational lens. By analogy to similar structures in high-redshift radio galaxies (where considerably more data is at hand), the first interpretation is deemed most likely. In this case, star formation rates of several hundred M_\odot per year are implied. If this rate of star formation lasts for a characteristic galaxian collapse time (\approx few times 10^8) yr, we are then witnessing the formation of a massive galaxy.

Finally, several of the QSOs have faint, spatially resolved (few arcsecond) sources of continuum and (probably) Ly α located within 100 kpc of the QSO. As described in the Appendix, these have $m_B \approx 23\text{--}24.5$ and $F_{\text{Ly}\alpha} \approx 10^{-16}$ ergs cm $^{-2}$ s $^{-1}$, and may be Ly α -emitting companion galaxies with Ly α luminosities of $\approx 10^{43}$ ergs s $^{-1}$ and UV continuum luminosities of few times $10^{44}\text{--}10^{45}$ ergs s $^{-1}$ (similar to but somewhat fainter than the four Ly α "companions" associated with the four high- z radio-loud QSOs discussed by Hu et al. 1990). Our candidates must be spectroscopically confirmed before being treated as bonafide QSO companion galaxies.

5.2. Implications

The data we have presented then have some implications for several important topics in extragalactic astronomy:

5.2.1. QSO and Radio Source Evolution

We have shown that high-redshift QSOs with strong radio emission are apparently immersed in highly gas-rich environments. The inferred total gas masses are comparable to the baryonic mass of a luminous galaxy. The estimated pressures are more than an order-of-magnitude larger than are inferred or measured around lower redshift, less powerful QSOs and radio galaxies. It is plausible to link this exceptional environment to the processes that both fuel the abundance of QSOs at high redshifts and confine and distort the accompanying radio sources.

5.2.2. Unification of Radio-loud QSOs and Radio Galaxies

The overall similarities between the Ly α and UV continuum structures of radio-loud QSOs and those of radio galaxies with similar redshifts and radio power implies that the radio galaxy and radio-loud QSO phenomena are intimately related. This is consistent with Barthel's (1989) "unification" scheme in which radio-loud QSOs and radio galaxies are drawn from the same population of objects but are viewed along and perpendicular to the radio source axis, respectively. Indeed, the Ly α /radio sidedness correlation offers us a chance to test the beaming model for one-sided radio jets. The data do not appear to be

consistent with models in which radio-loud QSOs evolve into radio galaxies. Evolution on time scales similar to the inferred radio source lifetimes ($\approx 10^7$ – 10^8 yr) is excluded if the Ly α nebulae are photoionized by the nucleus. This is because the recombination times in the QSO Ly α nebulae are so short (few hundred years) that the demise of the QSO will result in the quenching of the Ly α nebula on a light-crossing time ($\approx 10^5$ yr). This is at odds with the existence of similar Ly α nebulae in the high- z radio galaxies and QSOs. Models in which objects rapidly ($\ll 10^7$ yr) “flip-flop” between an active QSO phase and quiescent radio galaxy phase are excluded by the systematic differences between the large-scale radio sources of QSOs and radio galaxies (e.g., Barthel 1989).

5.2.3. Galaxy Formation and Early Evolution

Our data suggest that there are galaxies at redshifts of several with gas masses of $\approx 10^{11}$ – $10^{12} M_{\odot}$ and star-formation rates of several hundred M_{\odot} per year. These properties are certainly in accord with expectations for young/proto galaxies. The properties of the nebulae we infer from our data are remarkably similar to those predicted by Fall & Rees (1985) in their model for globular cluster formation in the two-phase medium of a protogalaxy. Indeed, the Fall & Rees model requires that a powerful ionization source be present to allow the cooling gas to “hang up” at 10^4 K long enough for a characteristic Jeans mass of $\approx 10^6 M_{\odot}$ to be “imprinted” upon it (see also Kang et al. 1990). This type of model then suggests that a QSO phase may be necessary for the formation of globular clusters. We wonder what role powerful QSOs at high redshifts play in the formation or early evolution of galaxies.

5.3. Future Directions

To explore these issues requires detailed investigation of the Ly α nebulae and UV fuzz associated with these QSOs. What is the dynamical state of the gas (is it being blown out by the QSO or could it be infalling or orbiting material)? What are the chemical properties of the gas (can we detect lines from heavy elements or might the gas be primordial)? What is the ionization state of the gas (this will allow us to refine our estimates of the gas density, pressure, mass, filling factor, etc.)? Does the radio/Ly α sidedness correlation persist when the

nebulae are imaged using emission lines less readily affected by dust? Can we find more cases like 3C 191 that allow us to relate the “associated” absorption-line systems to the Ly α nebulae? What is the overall spectral energy distribution of the “fuzz” (is it consistent with a stellar population or with scattered QSO light)? How do the detailed properties of the QSOs compare with those of the radio galaxies? How do the Ly α nebulae relate to the strong depolarization seen on the “counterjet” side in many high-redshift radio sources?

Related investigations of radio-quiet QSOs at high redshift are especially important. We now know that high-redshift radio galaxies and radio-loud QSOs live in extraordinary environments, and that there is an intimate connection between the radio source and this environment. However, it is unclear how to disentangle the lessons that the high- z radio galaxies and radio-loud QSOs teach us about the physics of extremely powerful radio sources from the lessons they teach about the formation and early evolution of galaxies and about the processes that drive the cosmic evolution of the entire QSO population (of which the radio-loud QSOs are a distinct minority). The arguments of Rees (1988) and others imply that high- z QSOs should generally be immersed in a dense two-phase gaseous halo (independent of their radio properties), and this gas should be detectable when irradiated by the powerful searchlight of the QSO. Is this really the case?

Partial financial support from a NATO research grant and from a visitor grant awarded to T. H. by the Netherlands Organization for Pure Research is gratefully acknowledged. W. v. B. acknowledges the support of IGPP, Lawrence Livermore. We thank Hy Spinrad for loaning us the narrow-band filters used for the Ly α imaging, and thank the staff at KNPO for their help in obtaining the data discussed in this paper. We also thank Eric Smith for providing us with the radial surface brightness software and instructing us in its use. Finally, we thank Peter Barthel, Ken Chambers, George Djorgovski, Andy Fabian, Mike Fall, Craig Foltz, Pat McCarthy, Colin Norman, Doug Richstone, and Ray Weymann for useful scientific input and Esther Hu and collaborators and Simon Garrington and collaborators for sending us copies of their related work in advance of publication.

APPENDIX

NOTES ON INDIVIDUAL OBJECTS

Q0017 + 154 (3C 9).—The Ly α emission is clearly elongated approximately N/S, misaligned with the triple radio source by $\sim 35^\circ$ (P.A. = 35° ; see Swarup, Sinha, & Saikia 1982). The nebula consists of a rather symmetric, oval-shaped region $8'' \approx 70$ kpc across, plus a possible faint filament extending another ≈ 30 kpc to the SE (coincident with the SE radio hotspot). The PSF in the Ly α frame has a faint “ghost” located $\approx 2''$ west of the peak. This is visible as a spurious western bulge in the Ly α CS frame shown in Figure 1. The QSO is unresolved in the U band image. Garrington, Conway, & Leahy (1990, hereafter GCL) find that 3C 9 is more strongly depolarized to the NW (counterjet side).

Q0109 + 176 (PKS 0109 + 176; 4C 17.09).—The Ly α nebula is quite asymmetric, extending at least $3'' \approx 26$ kpc west of the QSO. The radio source is strongly bent, with a series of bright knots (a jet?) to the east and a hotspot to the northwest (Barthel et al. 1988, hereafter BMSL). The QSO is unresolved in the U -band image. BTT find strong “associated” C IV absorption in this QSO.

Q0225 – 014 (PKS 0225 – 014; 4C 01.11).—The QSO is marginally resolved in Ly α . The PSS frame shows symmetric emission to the WNW and ESE of the QSO with a maximum size of $5'' \approx 43$ kpc. The radio source is a bent triple with hotspots to the SE and WNW of the nucleus (BMSL). GCP find much more Faraday depolarization to the SE (counterjet side). The QSO is also marginally resolved in the U image, with the spatially resolved continuum emission having a size and orientation similar to the Ly α emission.

Q0316 – 203 (MC 0316 – 203).—The QSO is unresolved in both the Ly α and B band images. Given our high success rate in resolving the Ly α in our sample of QSOs, it is suggestive that the radio source is also unresolved at the 0.5 level (BMSL). Hu et al. (1990) likewise found no evidence for discrete Ly α -emitting “blobs” near this QSO.

Q0445+097 (PKS 0445+097; 4C 09.17).—This is the most interesting QSO in our sample, and will be discussed in detail by Lehnert et al. (1990b). *Q0445+097* is easily resolvable in both the Ly α and *U* band frames. The Ly α nebula is asymmetric, with the bulk of the emission to the south and SW of the QSO. The overall size of the nebula is $\sim 12'' \approx 100$ kpc (see Fig. 2). The radio source is very asymmetric, with most (all?) of the radio emission to the WSW of the nucleus (BMSL). The morphology of the radio source suggests that the bright emission to the WSW of the QSO is a knotty jet. The spatially resolved structure in the *U*-band frame consists of a diffuse “fan” to the ESE and a possible fainter one to the SSW. BTT find strong “associated” CIV absorption in this QSO, and this system is discussed further in Lehnert et al. (1990b).

Q0549–213 (MC 0549–213).—Owing to an observing error, we inadvertently obtained a very deep (4200 s) *U* band image, but no Ly α image of this QSO! The QSO is definitely extended in the continuum, with a bright knot $\approx 1''$ to the NW of the QSO and a fainter fan or knot $\approx 4''$ to the WSW ($\approx 1''$ south of the solitary radio hotspot—see BMSL).

Q0730+257 (PKS 0730+257; 4C 25.21).—The Ly α is primarily located to the NW of the QSO, on the same side as the brighter radio emission and the knotty, one-sided radio jet (BMSL). The QSO is resolved in the *B* band image as well, despite rather mediocre seeing (1.8 FWHM). The continuum emission extends asymmetrically to the south and SE of the QSO.

Q0751+298 (B2 0751+298; 4C 29.27).—The Ly α and *U* band images of the QSO are both unresolved. It is interesting that the radio source is also very compact ($\approx 1''$; see BMSL).

Q0758+120 (MC5 0758+120).—The most morphologically spectacular Ly α nebula in our sample. The nebula is large ($13'' \approx 120$ kpc), with multiple plumes or filaments extending to the NW, SW, ESE, and ENE of the QSO. In contrast, the radio source is a simple triple source that is relatively straight and symmetric, with a roughly E/W orientation (BMSL). The *B* image of the QSO is unresolved.

Q0805+046 (4C 05.34).—The largest (130 kpc) and most luminous ($\approx 10^{45}$ ergs s $^{-1}$) Ly α nebula in our sample. The nebula is strongly asymmetric, with the bulk of the high-surface brightness emission arising from the SE side of the QSO. The radio source is also very asymmetric in the same sense (BMSL), and a knotty radio jet appears to join the nucleus to the bright SE radio hotspot. The QSO is resolved in the *B*-band image, with a roughly N/S orientation and the brightest extranuclear emission $\approx 1''$ north of the QSO. Note, however, that the continuum image is strongly contaminated by Ly α emission, and most of the structure within $\approx 3''$ SSE of the QSO is probably Ly α rather than continuum radiation. Thus, the properties of the UV “fuzz” in this QSO are particularly uncertain. There is also a diffuse continuum source with $m_B \approx 23$ located $\sim 7''$ south of the nucleus that coincides with a region of slightly enhanced Ly α emission ($F \approx 10^{-16}$ ergs cm $^{-2}$ s $^{-1}$). If it is really a companion galaxy to the QSO, it has a Ly α luminosity of $\approx 10^{43}$ ergs s $^{-1}$ and a UV continuum luminosity of $\approx 2 \times 10^{45}$ ergs s $^{-1}$.

Q0941+261 (B2 0941+261; OK 270).—The Ly α image reveals a complex, multimodal structure extending $\sim 10''$ (≈ 90 kpc) to the east of the QSO. The radio source is considerably smaller than the Ly α nebula, but exhibits the same orientation and asymmetry (it appears to consist of a core plus a one-sided, knotty, and strongly bent jet to the east; see BMSL). The *B*-band image of the QSO proper appears unresolved, but there are a number of faint ($m_B \approx 24$ to 24.5), diffuse objects $6''$ – $9''$ NE, E, SE, and SSE of the QSO. Two of these (the east and SE objects) coincide with very faint ($F \approx 5 \times 10^{-17}$ ergs cm $^{-2}$ s $^{-1}$) patches of Ly α emission. The overall impression (needing spectroscopic confirmation) is that the QSO is at the edge of (and interacting with?) a compact group of galaxies, some of which are Ly α emitters. If true, then the Ly α luminosities of the galaxies would be $\approx 5 \times 10^{42}$ ergs s $^{-1}$ and the UV luminosities $\approx 6 \times 10^{44}$ ergs s $^{-1}$.

Q1318+113 (PKS 1318+113; 4C 11.45).—Both the Ly α and *B* band images of the QSO are resolved. The bulk of the Ly α nebulosity is to the SSW of the QSO, on the same side as the bright, knotty radio jet and brighter radio hotspot. This side of the radio source is much less depolarized than the counterjet side (GCL). The structure in the *B* band has a diameter of $8''$ – $10''$, and a nearly E/W orientation. A detached “blob” is located $\approx 7.5''$ WNW of the QSO (nearly along the major axis of the fuzz surrounding the QSO; see Fig. 5). It has $m_B \approx 24$, implying that its UV luminosity is $\approx 3 \times 10^{44}$ ergs s $^{-1}$ if it is a true companion to the QSO.

Q1345+584 (4C 58.27).—There is asymmetric Ly α emission extending $\sim 6''$ (≈ 53 kpc) west of the QSO, on the same side as the bright, knotty, and strongly curved radio jet (BMSL). There is also excess Ly α emission (relative to the PSF) between radii of $\sim 1''$ and $3''$ north and south of the QSO. There were no bright, but unsaturated stars to determine the PSF in the *B* band frame, so we cannot comment on whether the QSO is resolved in the continuum.

Q1354+258 (PKS 1354+258).—The Ly α nebulae is somewhat asymmetric: the bulk of the emission arises to the east and south of the QSO, with the greatest extension to the South. The radio source (BMSL) is complex, consisting of a knotty, curved jet that exits the nucleus in P.A. $\approx -70^\circ$ and then curves strongly toward the southern radio hotspot. The two outer hotspots are oriented in P.A. $\approx 17^\circ$ (i.e., \approx perpendicular to the inner radio jet). It is therefore somewhat unclear how to count *Q1354+258* in the Ly α versus radio “sidedness” comparison. Insofar as the one-sided jet is apparently associated with the southern radio hotspot, and the Ly α is stronger to the south than to the north, this QSO follows the trend discussed in the text. On the other hand, the jet itself is brighter to the west of the QSO while the Ly α is brighter to the east. The *B*-band image of the QSO is marginally resolved, with a knot $\approx 1''$ NE of the QSO, and fainter material extending $\approx 5''$ to the NNE.

Q1658+575 (4C 57.29).—The Ly α nebula is rather round but may be slightly brighter and more extended to the NNE (the same direction as the one-sided, knotty radio jet; BMSL). The *B*-band image of the QSO is weakly resolved, with emission $\approx 1''$ – $2''$ to the east and fainter emission $\approx 10''$ in extent with a NNE/SSW orientation.

Q2150+053 (PKS 2150+053; 4C 05.81).—The Ly α emission is predominantly to the SSE of the QSO. The apparent Ly α “bulge” $\approx 3''$ to the WSW of the QSO is not real (it is the same “ghost” image noted above for *Q0017+154*, which was also observed through the 3662/60 filter). The radio source is a straight triple, with approximately an E/W orientation. Thus, there is no obvious radio/Ly α correspondence in *Q2150+053*. The QSO is just marginally resolved in the *U*-band image.

Q2222+051 (PKS 2222+051; 4C 05.84).—The Ly α emission is elongated in the NNE/SSW direction, with the brightest and most extended emission to the SSW. The radio source (BMSL) shares this morphology: the brighter radio hotspot is to the SW, and the radio map suggests the presence of a jet between the nucleus and SW hotspot. The *B*-band image of the QSO is unresolved.

Q2251 + 244 (PKS 2251 + 244).—The QSO is unresolved in both the Ly α and *B*-band images. The radio source is also subarcsec scale (BMSL). This QSO has a strong “associated” C IV absorption system (BTT).

Q2338 + 042 (PKS 2338 + 042; 4C 04.81).—The Ly α emission has a NW/SE orientation, with the emission brighter on the SE side. The radio source (BMSL) is a small, bent triple source with a bright hotspot to the SE and a fainter one to the west. The QSO is also well-resolved in the *B*-band frame, with the emission located primarily to the SE of the QSO and having a size of $\approx 6''$. However, the continuum image in Figure 5 is significantly ($\approx 30\%$) contaminated with Ly α emission, so that the properties of the resolved continuum source are particularly uncertain in this object. BTT have discovered a strong “associated” C IV absorption system in this QSO.

REFERENCES

- Adams, T. 1975, *ApJ*, 201, 350
 Barthel, P. 1989, *ApJ*, 336, 606
 Barthel, P., & Miley, G. 1988, *Nature*, 333, 319 (BM)
 Barthel, P., Miley, G., Schilizzi, R., & Lonsdale, C. 1988, *A&AS*, 73, 515 (BMSL)
 Barthel, P., Tytler, D., & Thomson, B. 1990, *A&AS*, 82, 339 (BTT)
 Baum, S., & Heckman, T. 1989a, *ApJ*, 336, 681
 ———. 1989b, *ApJ*, 336, 702
 Begelman, M., & Cioffi, D. 1989, *ApJ*, 345, L21
 Blandford, R., & Königl, A. 1979, *ApJ*, 232, 34
 Boroson, T., Persson, S. E., & Oke, J. B. 1985, *ApJ*, 293, 120
 Burstein, D., & Heiles, C. 1982, *AJ*, 87, 1165
 Carlberg, R. 1990, *ApJ*, 350, 505
 Carlberg, R., & Couchman, H. 1989, *ApJ*, 340, 47
 Cavaliere, A., & Padovani, P. 1988, *ApJ*, 333, L33
 Chambers, K. 1989, Ph.D. thesis, Johns Hopkins University
 Chambers, K., & Charlot, S. 1990, *ApJ*, 348, L1
 Chambers, K., & McCarthy, P. 1990, *ApJ*, 354, L9
 Chambers, K., Miley, G., & van Breugel, W. 1987, *Nature*, 329, 604
 Crawford, C., & Fabian, A. 1989, *MNRAS*, 239, 219 (CF)
 Crawford, C., Fabian, A., & Johnstone, R. 1988, *MNRAS*, 235, 183 (CFJ)
 di Serego-Alighieri, S., Fosbury, R., Quinn, P., & Tadhunter, C. 1988, *Nature*, 334, 591
 Djorgovski, S. 1988, in *Towards Understanding Galaxies at Large Redshifts*, ed. R. Kron & A. Renzini (Dordrecht: Kluwer), p. 259
 Djorgovski, S., Spinrad, H., McCarthy, P., & Strauss, M. 1985, *ApJ*, 299, L1
 Djorgovski, S., Strauss, M., Perley, R., Spinrad, H., & McCarthy, P. 1987, *AJ*, 93, 1318
 Fabian, A. 1989, *MNRAS*, 238, 41P
 Fall, S. M., & Rees, M. 1985, *ApJ*, 298, 18
 Fall, S. M., Pei, Y., & McMahon, R. 1989, *ApJ*, 341, L5
 Foltz, C., Chaffee, F., Weymann, R., & Anderson, S. 1988, in *QSO Absorption-Lines: Probing the Universe*, ed. J. C. Blades, D. Turnshek, & C. Norman (Cambridge: Cambridge University Press), p. 53
 Garrington, S., & Conway, R. 1990, preprint
 Garrington, S., Conway, R., & Leahy, P. 1990, preprint
 Garrington, S., Leahy, P., Conway, R., & Laing, R. 1988, *Nature*, 331, 147
 Heckman, T. M. 1990, in *Paired and Interacting Galaxies*, ed. J. Sulentic & W. Keel, in press
 Heckman, T. M., Armus, L., & Miley, G. K. 1990, *ApJS*, in press
 Heckman, T. M., Baum, S., McCarthy, P., & van Breugel, W. 1989, *ApJ*, 338, 48
 Heckman, T. M., Baum, S., & van Breugel, W. 1990, in preparation
 Hewitt, A., & Burbidge, G. 1987, *ApJS*, 63, 1
 Hu, E. 1988, in *Cooling Flows in Clusters and Galaxies*, ed. A. Fabian (Dordrecht: Kluwer Academic), p. 73
 Hu, E., & Cowie, L. 1987, *ApJ*, 317, L7
 Hu, E., Songaila, A., Cowie, L., & Stockton, A. 1990, preprint
 Ikeuchi, S. 1981, *PASJ*, 33, 211
 Kang, H., Shapiro, P., Fall, S. M., & Rees, M. 1990, *ApJ*, 363, 488
 Kapahi, V. K. 1990, in *Proc. NRAO Workshop on Parsec-Scale Jets*, in press
 Kennicutt, R. 1983, *ApJ*, 272, 54
 Koo, D., Kron, R., & Cudworth, K. *PASP*, 98, 285
 Krolik, J., & Kallman, T. 1988, *ApJ*, 324, 714
 Krolik, J., McKee, C., & Tarter, C. B. 1981, *ApJ*, 249, 422
 Laing, R. 1988, *Nature*, 331, 149
 Le Fevre, O., & Hammer, F. 1988, *ApJ*, 333, L37
 Lehnert, M., Heckman, T. M., Miley, G. K., & van Breugel, W. 1990a, in preparation
 Lehnert, M., Heckman, T., Chambers, K., Miley, G., & van Breugel, W. 1990b, in preparation
 Lilly, S. 1989, *ApJ*, 340, 77
 Mathews, W., & Ferland, G. 1987, *ApJ*, 323, 456
 McCarthy, P. 1988, Ph.D. thesis, University of California, Berkeley
 McCarthy, P., Spinrad, H., Djorgovski, S., Strauss, M., & van Breugel, W. 1987a, *ApJ*, 319, L39
 McCarthy, P., van Breugel, W., & Kapahi, V. 1990, *ApJ*, submitted
 McCarthy, P., van Breugel, W., Spinrad, H., & Djorgovski, S. 1987b, *ApJ*, 321, L29
 Meurs, E., & Fosbury, R. 1990, *ESO Workshop on Extranuclear Activity in Galaxies* (Garching bei München: European Southern Observatory)
 Miley, G. K. 1967, *Nature*, 218, 933
 ———. 1971, *MNRAS*, 152, 477
 ———. 1987, *IAU Symp.* 124, *Observational Cosmology*, ed. A. Hewitt, G. Burbidge, & L. Fang (Dordrecht: Reidel), p. 267
 Miller, J. 1989, in *Proc. IAU Symp.* 134, *Active Galactic Nuclei*, ed. D. Osterbrock and J. Miller (Dordrecht: Kluwer Academic), p. 273
 Norman, C., & Miley, G. K. 1984, *A&A*, 141, 85
 Neff, S., Hutchings, J., & Gower, A. 1989, *AJ*, 97, 1291
 Osterbrock, D. 1989, *Astrophysics of Gaseous Nebulae and Active Galactic Nuclei* (Mill Valley, CA: University Science Books)
 Osterbrock, D., & Mathews, W. 1986, *ARAA*, 24, 171
 Pedely, J., Rudnick, L., McCarthy, P., & Spinrad, H. 1989a, *AJ*, 97, 647
 ———. 1989b, *AJ*, 98, 1232
 Rees, M. 1988, *MNRAS*, 231, 91P
 Robinson, A., Binette, L., Fosbury, R., & Tadhunter, C. 1987, *MNRAS*, 227, 97
 Sarazin, C. 1986, *Rev. Mod. Phys.*, 58, 1
 Sargent, W., Boksenberg, A., & Steidel, C. 1988, *ApJS*, 68, 639
 Scheuer, P. A. G. 1974, *MNRAS*, 166, 513
 Schmidt, M., Schneider, D., & Gunn, J. 1986, *ApJ*, 310, 518
 Schneider, D., Gunn, J., Turner, E., Lawrence, C., Schmidt, M., & Burke, B. 1987, *AJ*, 94, 12
 Smith, E., Heckman, T., Bothun, G., Romanishin, W., & Balick, B. 1986, *ApJ*, 306, 64
 Soltan, A. 1982, *MNRAS*, 200, 115
 Spinrad, H. 1987, in *High Redshift and Primeval Galaxies*, ed. J. Bergeron, D. Kunth, B. Rocca-Volmerange, & J. Tran Thanh Van (Paris: Editions Frontières), p. 59
 Stockton, A., & MacKenty, J. 1987, *ApJ*, 316, 584
 Swarup, G., Sinha, R., & Saikia, D. 1982, *MNRAS*, 201, 393
 Tucker, W. 1977, *Radiation Processes in Astrophysics* (Cambridge: MIT Press)
 van Breugel, W., Heckman, T., Miley, G., Butcher, H., & Bridle, A. 1985, *ApJ*, 290, 496
 Wardle, J., & Miley, G. 1974, *A&A*, 30, 305
 Williams, R., Strittmatter, P., Carswell, R., & Craine, E. 1975, *ApJ*, 202, 296
 Zamorani, G., et al. 1981, *ApJ*, 245, 357

Note added in proof.—We have obtained long-slit spectra of five of the QSOs in this paper: Q0445+097, Q0758+120, Q0805+046, Q0941+261, and Q1318+113. These spectra confirm the presence of spatially extended Ly α emission whose properties are in good quantitative agreement with the results in the present paper. We have found, however, that the redshift of the spatially extended emission in Q0941+261 places it near the edge of the effective bandpass of the narrow-band filter used for our imaging. As a result, we estimate that the fluxes and luminosities of the spatially extended Ly α emission reported here for this QSO are probably systematically low by a factor of 2–3.